Geosystems and Geoenvironment 2 (2023) 100140

Contents lists available at ScienceDirect

Geosystems and Geoenvironment

journal homepage: www.elsevier.com/locate/geogeo

Geochemistry of volcanic rocks and dykes from the Remeshk-Mokhtarabad and Fannuj-Maskutan Ophiolites (Makran Accretionary Prism, SE Iran): New constraints for magma generation in the Middle East neo-Tethys

Emilio Saccani[a], Morteza Delavari[b], Asghar Dolati[b], Luca Pandolfi[c,d], Edoardo Barbero[a,e,*], Valentina Brombin[a], Michele Marroni[c,d]

[a] Dipartimento di Fisica e Scienze della Terra, Università di Ferrara, Ferrara 44123, Italy
[b] Faculty of Earth Sciences, Kharazmi University, Tehran 15719-19911, Iran
[c] Dipartimento di Scienze della Terra, Università di Pisa, Pisa 56126, Italy
[d] Istituto di Geoscienze e Georisorse, Consiglio Nazionale delle Ricerche (CNR), Pisa 56124, Italy
[e] Istituto di Geoscienze e Georisorse, Consiglio Nazionale delle Ricerche (CNR), Torino 10125, Italy

ARTICLE INFO

Article history:
Received 27 June 2022
Revised 29 August 2022
Accepted 30 September 2022

Keywords:
Ophiolite
Geochemistry
Petrology
Oceanic crust
Makran Accretionary Prism
Early Cretaceous
Iran

ABSTRACT

The Remeshk-Mokhtarabad and Fannuj-Maskutan ophiolites represent two major ophiolitic units in the North Makran Domain (Makran Accretionary Prism). Volcanic rocks and dykes of these ophiolites mainly consist of basalts and rare basaltic andesites, andesites and dacites. No chemical distinction can be seen in basalts from these two ophiolitic units, or between volcanic rocks and dykes. Basaltic rocks show a broad MORB-type nature but variable chemical composition (e.g., SiO_2= 42.64–52.63 wt%; TiO_2= 0.98–2.43 wt%; Mg# = 71–50). They show both N-MORB (Type 1) and E-MORB (Type 2) compositions (MORB: mid-ocean ridge basalt; N: normal; E: enriched). Type 1 rocks are very rare in both ophiolitic units, whereas Type 2 rocks are predominant. Type 1 rocks show low Th (0.10–0.16 ppm), Nb (1.86–2.82 ppm), Ta (0.09–0.17 ppm) abundance and low $(La/Yb)_N$ (0.50–0.75), $(La/Sm)_N$ (0.48–0.72) ratios. Compared to N-MORBs, Type 2 basalts show slight enrichment in Th (0.42–1.60 ppm), Nb (6.09–14.6 ppm), and Ta (0.227–0.792 ppm), as well as $(La/Yb)_N$ and $(La/Sm)_N$ ratios >1 like those observed in typical E-MORB. Trace element petrogenetic models indicate that primitive basalts derived from partial melting of a heterogeneous sub-oceanic mantle variably metasomatized by plume-type (OIB-) components. Type 1 basalts derived from partial melting of mantle regions with no enrichment in OIB-type components, whereas Type 2 basalts derived from partial melting of DMM sources variably enriched by OIB-components. These rocks formed in an oceanic basin that was strongly affected by mantle plume activity and different extents of plume-ridge interaction.

1. Introduction

The Alpine-Himalayan belt is made up of a complex network of orogenic belts, suture zones, and microcontinental blocks extending from the western Mediterranean area to the Himalayan belt (Dercourt et al., 1986; Şengör, 1990; Ricou, 1994; Stampfli and Borel, 2002; Barrier et al., 2018). The Makran Accretionary Prism (SE Iran-SW Pakistan) represents the central segment of the Alpine-Himalayan belt, connecting the Zagros and the eastern Mediterranean belts, to the west, and the Pakistani-Himalayas belt, to the east (Fig. 1a). It is one of the widest and long-lasting accretionary prisms on Earth (e.g., Kopp et al., 2000). Its formation started not later than the Late Cretaceous in consequence of the subduction of the Neo-Tethys below the Lut and Afghan blocks, which is still active offshore in the Oman Sea (Fig. 1a). The Makran Accretionary Prism includes several ophiolitic and metaophiolitic units representing different portions of

* Corresponding author at: Dipartimento di Fisica e Scienze della Terra, Università di Ferrara, 44123 Ferrara, Italy.
E-mail addresses: sac@unife.it (E. Saccani), delavari@khu.ac.ir (M. Delavari), dolati@khu.ac.ir (A. Dolati), luca.pandolfi@unipi.it (L. Pandolfi), edoardo.barbero@igg.cnr.it (E. Barbero), brmvnt@unife.it (V. Brombin), michele.marroni@unipi.it (M. Marroni).

https://doi.org/10.1016/j.geogeo.2022.100140

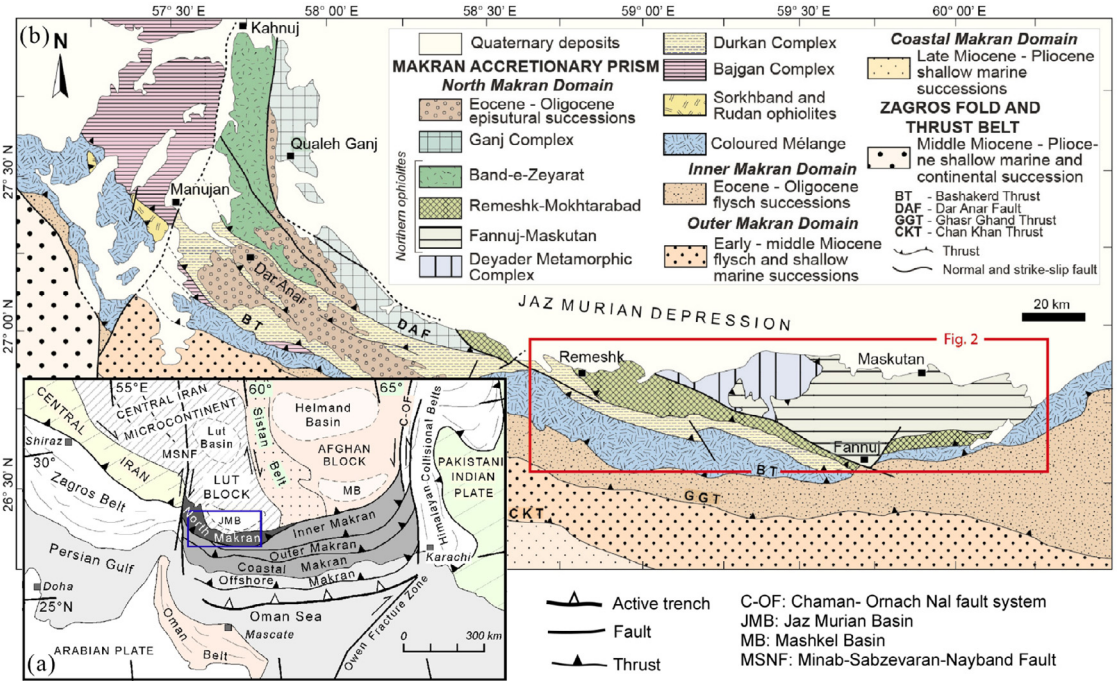

Fig. 1. (a) Simplified tectonic sketch map of the Iranian-Afghan-Pakistani area (modified from Khan et al., 2007; Allahyari et al., 2014; Mohammadi et al., 2016; Pirnia et al., 2020); (b) simplified geological map of the North Makran Domain showing the different tectono-stratigraphic units (modified from Eftekhar-Nezhad et al., 1979; Samimi Namin, 1982, 1983; Burg, 2018; Barbero, 2021). Box in panel (a) show the area expanded in panel (b). Box in Panel (b) indicate the area shown in Fig. 2.

the Mesozoic Neo-Tethys in the Makran sector, including ocean floor lithosphere and seamounts, as well as volcanic arc margins (Burg, 2018; Barbero et al., 2020a, 2020b, 2021a; Pandolfi et al., 2021; Moghadam et al., 2022). Therefore, this accretionary complex is an outstanding natural laboratory for understanding the mechanisms of oceanic formation and the evolution of subduction zones.

After pioneering works carried out in the 1970s and 1980s (Delaloye and Desmons, 1980; McCall and Kidd, 1982; McCall, 1983, 1985a, 1985b, 1985c, 1997; Desmons and Beccaluva, 1983), the Makran ophiolites have been overlooked for many years, apart from a few scattered works (Ghazi et al., 2004; Dolati 2010; Shahabpour, 2010). Increasing extensive research carried out in the last decade on the Mesozoic ophiolites and metaophiolites in the North Makran Domain (Fig. 1a, b) have improved our comprehension of the various geodynamic environments in which these ophiolites were born, evolved, and were finally accreted to the southern margin of the Lut Block (e.g., Dolati and Burg, 2013; Hunziker, 2014; Hunziker et al., 2015, 2017; Moslempour et al., 2015; Mohammadi et al., 2016; Dorani et al., 2017; Burg, 2018; Saccani et al., 2018; Monsef et al., 2019; Barbero et al., 2020a, 2020b, 2021a, 2021b; 2021c; Esmaeili et al., 2020, 2021; Sepidbar et al., 2020; Barbero, 2021; Pandolfi et al., 2021; Moghadam et al., 2022).

The Remeshk-Mokhtarabad and Fannuj-Maskutan ophiolites cropping out in the inner North Makran Domain have previously been considered, together with the Ganj Complex, the Band-e-Zeyarat ophiolites, and the Deyader Complex as the so-called "northern ophiolites" (Fig. 1b), which are separated from the southern Sorkhband-Rudan ophiolites and the ophiolitic mélange (Coloured Mélange) by the Bajgan-Durkan Complex (McCall, 2002; Hunziker, 2014; Burg, 2018). Previous interpretations have suggested that the Bajgan-Durkan Complex represents the remnants of a continental ribbon located between the northern and southern Makran ophiolites (e.g., McCall, 2002; Burg, 2018). The Jurassic magmatic rocks within the Bajgan-Durkan Complex have been assumed to be produced by rift magmatism associated with rifting and separation of the Bajgan-Durkan continental ribbon from the southern margin of the Lut Block (Hunziker et al., 2015). Geochemical data have shown that the intrusive and extrusive sequences of the Remeshk-Mokhtarabad and Fannuj-Maskutan ophiolites consist of normal (N-) and enriched (E-) types mid-ocean ridge basalts (MORB), which have been interpreted, together with other Makran northern ophiolites, as representative of a backarc basin located between the Lut Block, to the north, and the Bajgan-Durkan continental ribbon, to the south (Hunziker, 2014; Moslempour et al., 2015; Khalatbari-Jafari et al., 2016; Burg, 2018; Sepidbar et al., 2020). However, this tectonic interpretation of the Remeshk-Mokhtarabad and Fannuj-Maskutan ophiolites was strongly influenced by the interpretation of the Bajgan-Durkan as a continental ribbon, which fostered interpretations aimed at reconciling the broad MORB affinity of such rocks with the existence of a marginal basin beyond the Bajgan-Durkan continental ribbon. Nonetheless, rocks of MORB affinity commonly occur at mid-oceanic ridges, but also in within-plate seamounts, at convergent margins, and in continental rifts (Dilek and Furnes, 2011; Saccani, 2015; Saccani et al., 2017).

Recent structural, petrological, biostratigraphic, and geochronological studies have shown that, in contrast to previous interpretations, the Ganj Complex represents remnants of a volcanic arc (Barbero et al., 2020a); the Durkan Complex consists of volcano-sedimentary successions which are remnants of oceanic seamounts (Barbero et al., 2021a; 2021b); the Bajgan Complex consists of metaophiolites whose protoliths were formed in a Late Jurassic–Cretaceous oceanic basin characterized by mantle plume activity and plume-ridge interaction (Barbero et al., 2021c; Pandolfi et al., 2021). In addition, a similar tectono-magmatic setting of formation has been suggested for the Band-e-Zeyarat and Deyader ophiolites (Barbero et al., 2020b; Saccani et al., 2022). Given this evidence, the interpretation of the origin of the Remeshk-Mokhtarabad and Fannuj-Maskutan ophiolites in a backarc basin is now arguable and it should be re-discussed in the light of the recent findings. Ophiolitic magmatic rocks show wide variations in composition, which

are generally attributed to variable source compositions and contributions from multiple components. This is particularly effective for volcanic rocks and dykes, as they commonly represent the composition of true magmatic liquids. Compositional variations in the source region are, in turn, closely related to the geodynamic evolution of oceanic basins. In fact, geochemical fingerprinting of ophiolitic volcanic rocks and dykes is widely used to reconstruct the geochemical and magmatic processes responsible for building the oceanic lithosphere in different geodynamic settings (Pearce, 2008; Saccani, 2015). This paper is, therefore, focused on volcanic rocks and dykes from the Remeshk-Mokhtarabad and Fannuj-Maskutan ophiolites. We present new whole-rock geochemical data on these rocks with the aims of a) defining their petrogenetic processes; b) providing robust constraints about the geochemical nature of the oceanic lithosphere in which they were formed; c) assessing their tectono-magmatic significance within the Makran sector of the Neo-Tethys also through a geochemical comparison with other North Makran ophiolitic and metaophiolitic units. A new definition of the nature of the oceanic lithosphere in which the Remeshk-Mokhtarabad and Fannuj-Maskutan ophiolites were formed will also provide new constraints for regional scale reconstructions of the geodynamic evolution of the Makran Neo-Tethys.

2. Geological setting

2.1. General geological setting of the Makran Accretionary Prism

The Makran is a well-known accretionary complex developed during the Cretaceous to present-day northward subduction of the Neo-Tethyan oceanic lithosphere beneath the Lut and Afghan blocks (e.g., McCall and Kidd, 1982; Dercourt et al., 1986; Glennie et al., 1990; Mohammadi et al., 2016; Burg, 2018; Saccani et al., 2018; Monsef et al., 2019; Esmaeili et al., 2020; Barbero et al., 2020a, 2021a, 2021c; Pandolfi et al., 2021; Moghadam et al., 2022). The structural setting of the Makran Accretionary Prism and its relationships with the main tectonic domains of the Iran–Pakistan–Arabia area is shown in Fig. 1a. In the Iranian sector, the Makran Accretionary prism extends, from north to south, from the Jaz Murian depression in south Iran to the offshore Makran in the Oman Sea (Fig. 1a), which represents the present-day deformation front of the accretionary prism (McCall and Kidd 1982; Dercourt et al., 1986; Burg et al., 2008, 2013). The onshore Makran Accretionary Prism is characterized by the tectonic juxtaposition of several tectono-stratigraphic domains (Dolati, 2010; Burg et al., 2013; Figs. 1a, b). These domains are from the structural top to the bottom (from north to south): (1) the North Makran; (2) the Inner Makran; (3) the Outer Makran; (4) the Coastal Makran (Fig. 1a). The Inner, Outer, and Coastal Makran Domains represent the post-Eocene accretionary complex, whereas the North Makran Domain represents remnants of the pre-Eocene accretionary prism (e.g., Dolati, 2010; Burg et al., 2013; Dolati and Burg, 2013; Burg, 2018; Esmaeili et al., 2020). The North Makran Domain consists of a tectonic stack of lithostratigraphic units formed in both Cretaceous volcanic arc and Jurassic-Cretaceous oceanic lithosphere settings (e.g., McCall, 1997; Ghazi et al., 2004; Hunziker et al., 2015; Mohammadi et al., 2016; Saccani et al., 2018; Esmaeili et al., 2020; Barbero et al., 2021b, Pandolfi et al., 2021; Moghadam et al., 2022).

The North Makran includes (from the higher to the lowermost structural position; Fig. 1b): (1) the Ganj Complex; (2) the Northern Ophiolites; (3) the Deyader and Bajgan Metamorphic Complexes; (4) the Durkan Complex; (5) the Sorkhband–Rudan tectonic slices; (6) the Coloured Mélange Complex. The Sorkhband–Rudan ophiolites and the Coloured Mélange Complex are also known as the Southern Ophiolites (Delavari et al., 2016; Moghadam et al., 2022). Some of these units show variable degrees of metamorphic imprint, ranging from low-grade greenschist facies conditions in some sequences of the Durkan Complex (Barbero et al., 2021a, 2021b) to blueschist facies conditions in the Bajgan (McCall, 2002; Dorani et al., 2017; Pandolfi et al., 2021) and Deyader (Hunziker et al., 2017; Bröcker et al., 2021) Complexes. Ophiolites and metaophiolites are largely prevailing in the North Makran, whereas volcanic arc rocks are limited to the Ganj Complex, which represents fragments of a Late Cretaceous volcanic arc that was likely built up close to the southern margin of the Lut Block (Barbero et al., 2020a). Blocks and slices of volcanic arc rocks showing both Early and Late Cretaceous age are also included in the Coloured Mélange Complex (Saccani et al., 2018).

The Northern Makran ophiolites are distinguished in three distinct ophiolitic units (Fig. 1b; McCall and Kidd, 1982) including, from west to east: (1) the Band-e-Zeyarat/Dar Anar; (2) the Remeshk-Mokhtarabad; (3) the Fannuj-Maskutan. These ophiolitic units share the same lithostratigraphic features including a fragmented magmatic suite with ultramafic cumulates, cumulate gabbros, high-level isotropic gabbros, plagiogranites, a sheeted dike complex, and pillow lavas. These rocks are associated with Early Cretaceous pelagic sediments (McCall, 2002; Ghazi et al., 2004; Dolati, 2010; Hunziker et al., 2015; Moslempour et al., 2015; Burg, 2018; Barbero et al., 2020b; Sepidbar et al., 2020).

The Deyader Metamorphic Complex is overthrust by the North Makran ophiolites (Fig. 1b). It consists of a low-grade metamorphic complex with metaophiolites that have experienced high pressure-low temperature (HP-LT) metamorphism (McCall, 2002; Hunziker et al., 2015, 2017). Geochemical data show that the magmatic protoliths of these rocks were consisting of sub-alkaline basalts showing both N-MORB and E-MORB compositions, as well as transitional basalts showing plume-type MORB (P-MORB) composition. It has been suggested that these protoliths represent fragments of a Late Jurassic – Cretaceous oceanic basin that was strongly affected by mantle plume activity and different extents of plume-ridge interaction (Saccani et al., 2022).

The Bajgan and Durkan complexes were previously assumed to collectively represent the remnants of a continental ribbon separated from the Lut Block in the Jurassic (e.g., McCall and Kidd, 1982; McCall, 2002; Hunziker et al., 2015). However, recent studies have shown that the Bajgan Complex shares many features with the Deyader Complex. In fact, it consists of Late Jurassic to Early Cretaceous meta-ophiolites and related pelagic metasediments that were affected by low- to medium-pressure/low-temperature metamorphism that reached the blueschist metamorphic facies in the Late Cretaceous (Pandolfi et al., 2021). Similar to the Deyader Complex, the Bajgan Complex is structurally overthrust by the North Makran ophiolites (Fig. 1b) and magmatic protoliths include cumulitic ultramafic and mafic rocks, isotropic gabbros, plagiogranites, volcanic, and volcaniclastic sequences ranging in composition from N-MORB to E-MORB affinities and alkaline ocean-island basalt (OIB) chemistry. Petrogenetic studies have shown that magmatic protoliths were formed at both mid-ocean ridge and seamount settings in an oceanic basin characterized by mantle plume activity and plume–ridge interaction processes (Barbero et al., 2021c; Pandolfi et al., 2021). Accordingly, recent studies have shown that the Durkan Complex consists of Early Cretaceous to Paleocene metapelites, carbonates and volcanic successions which have been interpreted as remnants of oceanic seamounts (Barbero, 2021; Barbero et al., 2021a, 2021b).

The Sorkhband and Rudan ophiolites crop out within the shear zone between the Coloured Mélange and the Bajgan Complex (McCall, 2002; Delavari et al., 2016; Fig. 1b). The Sorkhband ultramafic complex contains dunites, harzburgites, and chromitites with interlayered dunites, as well as clinopyroxenites. Depleted harzburgites are the dominant rock-type (Delavari et al., 2016), though stratiform chromitites with interlayered dunites are common.

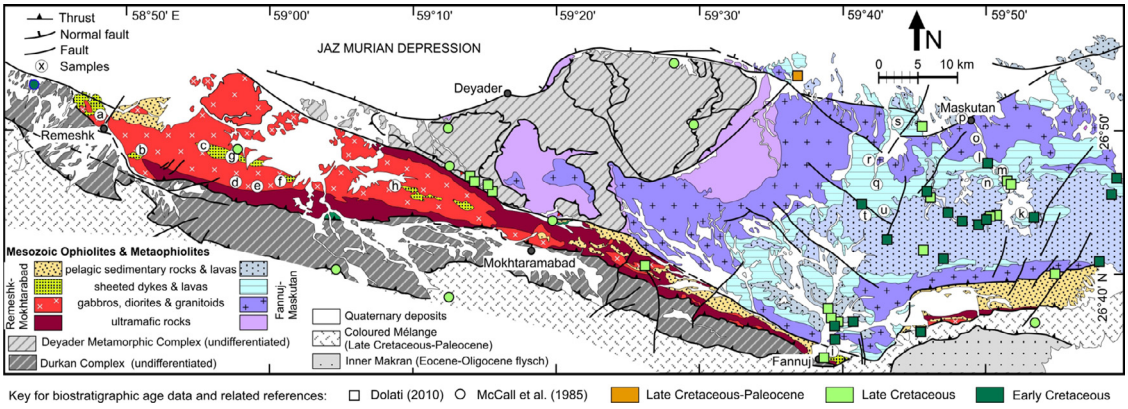

Fig. 2. Simplified geological map of the Remeshk-Mokhtarabad and Fannuj-Maskutan ophiolites, and surrounding tectonic units (modified from Hunziker et al., 2017; Burg, 2018 based on our field work). Sampling locations are identified in Figure with short labels. The correspondence between samples and short labels is given in Supplementary Data, Table S1. Schematic biostratigraphic data on the North Makran ophiolitic and metaophiolitic units are also shown.

Based on Cr-spinel chemistry, Moghadam et al. (2022) have suggested that the Sorkhband ultramafic complex formed in a supra-subduction zone setting characterized by low-Ti and very low-Ti (boninite) melts.

The Coloured Mélange Complex is the southernmost and structurally lowermost unit in the North Makran (Fig. 1b). It consists of tectonic slices of serpentinites, pillow lavas, pelagic limestones, radiolarites, and distal turbidites. It is suggested to have formed in the trench of a North-dipping subduction zone by scraping off fragments of both the subducting oceanic plate and the upper plate (i.e., volcanic arc) during Late Cretaceous to Early Paleocene times (McCall and Kidd, 1982; McCall, 2002; Burg, 2018; Saccani et al., 2018; Esmaeili et al., 2020, 2021). Biomicrites intercalated with pillow lavas contain Late Cretaceous microfaunas (McCall, 2002), whereas the radiolarites associated with pillow lavas range from Early to Late Cretaceous (Saccani et al., 2018).

2.2. Geological setting of the Remeshk-Mokhtarabad and Fannuj-Maskutan ophiolites

The Remeshk-Mokhtarabad ophiolitic unit is exposed in a fault-bounded synform (Burg, 2018) that stretches from Remeshk, to the west, to Fannuj, to the east (Fig. 2), whereas the Fannuj-Maskutan ophiolites represent the easternmost ophiolitic unit in the North Makran. They crop out between Fannuj, to the south, and Maskutan, to the north. Klippen of ultramafic rocks to the south of Deyader and along the faulted border with the Jaz Murian depression (Fig. 2) are interpreted as belonging to this ophiolitic Unit (Hunziker, 2014; Burg, 2018). The geological settings of the Remeshk-Mokhtarabad and Fannuj-Maskutan ophiolites have been described in detail by many authors (Desmons and Beccaluva, 1983; McCall et al., 1985; McCall, 2002; Hunziker, 2014; Hunziker et al., 2015; Moslempour et al., 2015; Khalatbari-Jafari et al., 2016; Burg, 2018; Sepidbar et al., 2020). From these works, it results that the Remeshk-Mokhtarabad and Fannuj-Maskutan ophiolites, though with some minor differences, show very similar lithostratigraphic and geochemical features. Both these ophiolitic units show the typical sequences of an ophiolite, including (Fig. 2): (1) ultramafic rocks at the base, mainly consisting of serpentinized peridotites representing the upper mantle sequence. This sequence is topped by a dunitic mantle-crust transition zone; (2) an intrusive sequence starting at the bottom with a layered lower crust sequence passing upward to upper level gabbros with minor plagiogranite intrusions, dykes, and veins (Fig. 3a); (3) a sheeted dykes complex (Fig. 3b-d); (4) an extrusive sequence (Fig. 3b, e-h) topped, in turn, by deep-marine sedimentary rocks.

The peridotites in the upper mantle section consist of lherzolites, clinopyroxene-bearing -harzburgites, and dunites, which include podiform chromitite (Moslempour et al., 2015; Burg, 2018). The Fannuj-Maskutan ophiolites are characterized by a huge mantle-crust transition zone that reaches ~1000 m in thickness (Burg, 2018). The crustal sequence is widely exposed in both ophiolitic units (Fig. 2). The lower intrusive sequence consists of layered olivine gabbros, troctolites, pegmatitic olivine gabbros, anorthosites, and wehrlites. The upper crust gabbro intrusions mainly consist of isotropic gabbros and coarse-grained gabbros and subordinate diorites, trondhjemites, and plagiogranites. The sheeted dyke sequence is exposed in the neighbourhoods of Remeshk and over a wide area between Fannuj and Maskutan. Dykes in the sheeted dykes show thicknesses ranging from about 10 cm to a couple of metres (Fig. 3b-d). Volcanic rocks basically occur as pillow (Fig. 3a, e) and massive lava flows (Fig. 3h), though very minor tuffs are locally found. Pillows range in size from a few decimetres to 1 m (Fig. 3a, e), whereas massive lava flows range in size from about one meter to several metres (Fig. 3f). In general, the sheeted dyke-volcanic sequences in the Remeshk-Mokhtarabad ophiolites are thinner than those of the Fannuj-Maskutan ophiolitic unit (Burg, 2018). Nonetheless, our field investigations indicate that outcrops of these sequences are wider than what was described by Burg (2018) and form outcrops that can be followed for some kilometers. Volcanic rocks and dykes are mainly consisting of basalts and minor basaltic andesites, andesites, dacites, and rhyolites. In both ophiolitic units, individual dykes of variable nature (from basalt to rhyolite) and variable size (from a few decimetres to a few metres) crosscut all sequences but are particularly abundant in the upper crust gabbros (Fig. 3a) and the volcanic sequence. Both pillow and massive lavas commonly include thin and discontinuous layers of pelagic marls and limestones (Fig. 3g, h). Frequently, pelagic sedimentary rocks interbedded within pillow and massive lavas show soft-sediment deformations (Fig. 3g) suggesting that lava flows were emplaced onto weakly consolidated sediments. According to Hunziker (2014), isotopic and chemical compositions of volcanic rocks and dykes indicate N-MORB and E-MORB affinities. Nd isotopic compositions of mafic rock types indicate that the Remeshk-Mokhtarabad and Fannuj-Maskutan ophiolites were produced by the same relatively primitive E-MORB type magma type (Hunziker, 2014).

The ophiolitic sedimentary cover consists of red to pink, fine-grained limestones and radiolarian shales, grey micritic limestones, and red to brown cherts. In both the Remeshk-Mokhtarabad and Fannuj-Maskutan ophiolitic units, the oldest dated sedimentary rocks on the top of N-MORB and E-MORB pillow-lavas are pelagic

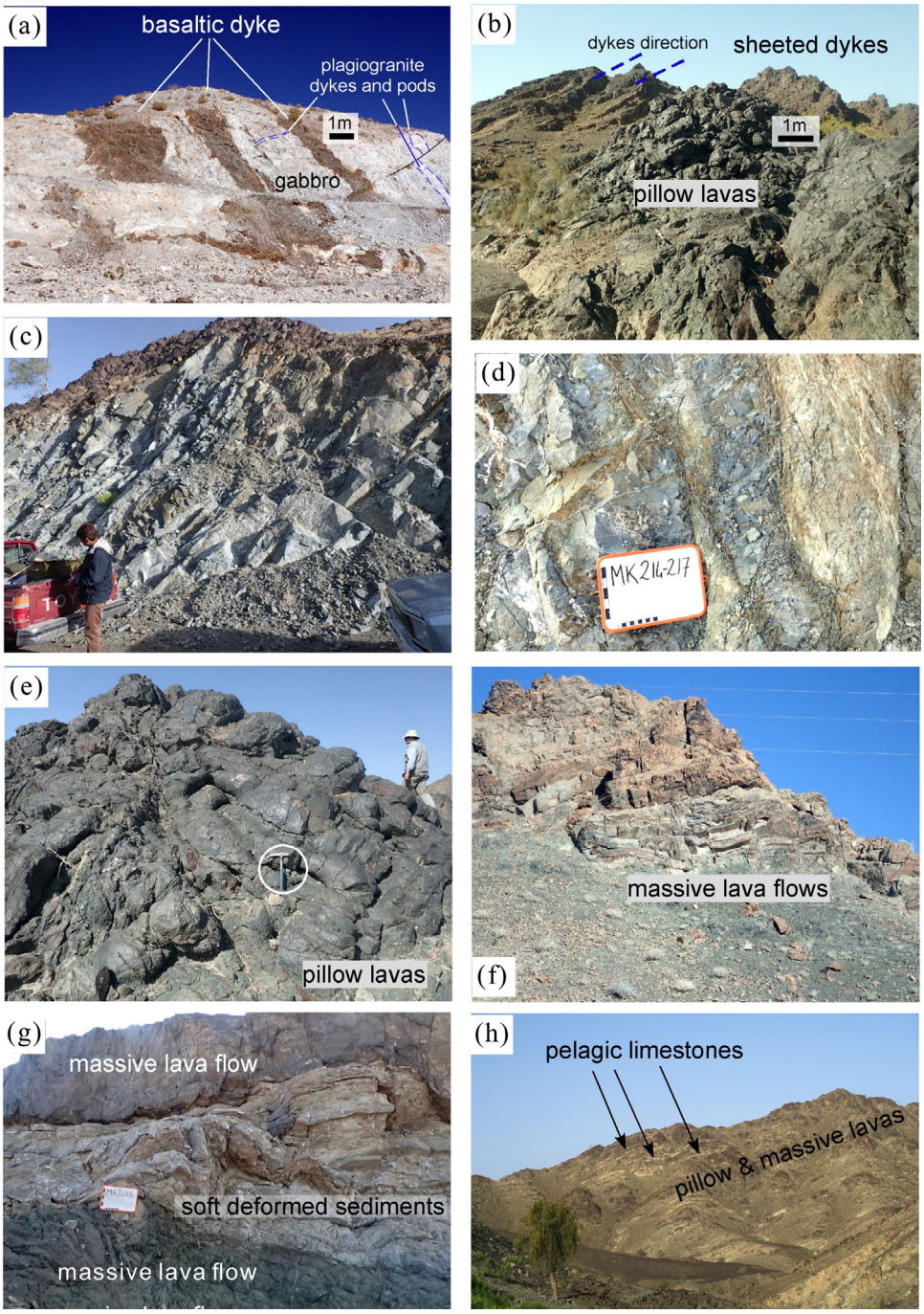

Fig. 3. Field photographs of the different rock types in the Remeshk-Mokhtarabad and Fannuj-Maskutan ophiolites. (a) basaltic and plagiogranite dykes cutting the upper part of the gabbro sequence; (b) sheeted dykes overlain by pillow lavas; (c, d) sheeted dykes with dykes of different size and composition (c: large view, d: close view); (e) pillow lavas; (f) massive lava flows; (g) close view of soft-sediment deformations within pelagic marly limestone bed sandwiched between massive lava flows; (h) large view of a volcanic sequence with alternating massive lavas, pillow lavas and beds of pelagic limestone. Photo in a) was taken in the Remeshk-Mokhtarabad unit; photos in (b-h) were taken in the Fannuj-Maskutan unit.

limestones and hemipelagic red marls containing nannofossils not younger than Barremian (ca. 130–125 Ma). This sequence is covered by Upper Cretaceous shallow water limestone unconformably in the eastern part (Dolati, 2010; Fig. 2). Minor alkaline lavas were dated at ca 120 Ma (Shahabpour, 2010).

The Fannuj-Maskutan ophiolitic unit is unconformably covered by Maastrichtian shallow-water limestones and, locally, turbiditic series interbedded with andesitic lava flows, which are lacking in the Remeshk-Mokhtarabad ophiolites. These lavas show a calc-alkaline type geochemistry (Desmons and Beccaluva, 1983; Hunziker, 2014), which has been associated with a subduction-related origin. The occurrence of post-Maastrichtian subduction-related magmatism supports previous interpretations, which have dated the beginning of subduction as Cretaceous (e.g., Delaloye and Desmons, 1980; Desmons and Beccaluva, 1983; Hunziker, 2014; Saccani et al., 2018; Barbero et al., 2020a). Both

Remeshk-Mokhtarabad and Fannuj-Maskutan ophiolites are topped by unconformable Eocene-Oligocene proximal turbiditic successions (McCall, 1985a; Dolati, 2010).

3. Sampling and petrography

Because the scope of this paper is to study the petrogenetic processes that were responsible for the formation of the oceanic crust of the Makran Neo-Tethys, sampling was focused on the volcanic rocks and dykes. In fact, the compositions of these rocks most likely represent magmatic liquid compositions and can, therefore, reliably be used for petrogenetic studies (e.g., Pearce and Norry, 1979; Pearce, 2008; Saccani, 2015). A total of forty-two samples (fifteen samples from the Remeshk-Mokhtarabad ophiolites and twenty-seven samples from the Fannuj-Maskutan ophiolites) are studied in this paper. In both the ophiolitic units, we sampled all the volcanic and dyke varieties including pillow and massive lavas, dykes from the sheeted dyke complex, and individual dykes cutting the intrusive sequence. Sample types and sampling localities are shown in Fig. 2 and Supplementary Data (Table S1).

Most of the studied rocks are affected by low-grade ocean-floor hydrothermal alteration, which resulted in different extent of replacement of the primary igneous phases, whereas the primary igneous textures are always well preserved. Olivine is rarely preserved, as it is commonly replaced by iddingsite or chlorite. Fresh plagioclase is rare, since it is usually replaced by albite + calcite assemblages and, locally, by albite + epidote assemblages. Clinopyroxene alteration normally occurs as pseudomorphic replacement by actinolitic-tremolitic amphibole or, rarely, by chlorite. Nonetheless, fresh clinopyroxene relics are locally observed in some coarse-grained dykes. Volcanic glass in the groundmass is commonly altered to chlorite. However, in a few samples volcanic glass is devetrified to a cryptocrystalline assemblage. Few pillow lava samples exhibit amygdaloidal textures, with vesicles filled by calcite and, subordinately, by chlorite and zeolite. In addition, small calcite veins are frequent in pillow lavas. In contrast, very few dyke samples display small quartz veins. Regardless of the secondary mineralogical transformations, the following petrographic description will be made on the bases of the primary igneous phases.

Massive lava flows mainly show aphyric texture. The groundmass commonly ranges from subophitic-intergranular (Fig. 4a) to subophitic-intersertal (Fig. 4b) with plagioclase laths and granular interstitial clinopyroxene or with plagioclase laths partially enclosed within clinopyroxene crystals and interstitial Fe-Ti oxides. The groundmass grain-size is variable, from very fine-grained (0.2 mm; Fig. 4b) to medium-grained (0.5–0.7 mm; Fig. 4a). Plagioclase and clinopyroxene show comparable abundance in basaltic rocks (Fig. 4a), whereas plagioclase is largely predominant in andesites, which also show weakly porphyritic textures (PI ~10) with plagioclase, olivine, and clinopyroxene phenocrysts (Fig. 4c). In contrast, massive lavas with differentiated composition display hypocrystalline texture with intersertal, very small plagioclase laths set in altered glass.

Pillow lavas show a wide range of textures. They include both aphyric and weakly porphyritic and glomeroporphyritic (PI = 10-20) textures. Some porphyritic samples are characterized by microphenocrysts of plagioclase, whereas other samples show large plagioclase phenocrysts together with minor olivine and Fe–Ti oxide micro-phenocrysts. The groundmass ranges from microcrystalline to hypocrystalline and cryptocrystalline. The subophitic-intersertal texture is largely prevailing and is characterized by small laths of plagioclase and interstitial clinopyroxene or volcanic (Fig. 4d) glass plus, eventually, Fe–Ti oxides. Nonetheless, intergranular texture is locally observed. Very few samples show variolitic texture with fans of diverging plagioclase and clinopyroxene in the interstices. The groundmass grain-size is commonly fine-grained (<0.5 mm); however, samples where plagioclase is relatively more abundant (e.g., basaltic andesites) show coarse-grained texture. Basaltic dykes, either individual or sheeted dykes, mainly show coarse-grained doleritic texture (crystals averaging 1–2 mm in size), though medium to fine-grained (crystals averaging <0.5 mm in size) holocrystalline textures are locally observed.

Commonly, the dykes are characterized by subophitic texture with plagioclase laths partially enclosed within clinopyroxene crystals (Fig. 4e), as well as interstitial Fe–Ti oxides and rare altered olivine crystals. Some samples show poikilitic texture with plagioclase laths enclosed in clinopyroxene oikocrysts (Fig. 4f). Normally, dykes show equigranular texture, but a few samples are inequigranular, with very large and zoned plagioclase crystals (Fig. 4e). Zoned plagioclase can also be found in a few other samples. Dyke MK174 is the only sample showing holohyaline texture with glass devetrified to a pale brown cryptocrystalline mineral assemblage. The mineral assemblage in dykes is dominated by the ubiquitous presence of plagioclase and clinopyroxene accompanied by variable amounts of Fe–Ti oxides. In a couple of dykes from the sheeted dyke sequence, fresh clinopyroxene relics can be seen. In all the studied samples, the crystallization order is olivine + plagioclase + clinopyroxene + Fe–Ti oxides, which is the typical crystallization order of MORB-type rocks, as well as many alkaline basalts (Beccaluva et al., 1983).

4. Analytical methods

Whole rock major and some trace elements were analysed by X-ray fluorescence (XRF) on pressed-powder pellets, using an ARL Advant-XP automated X-ray spectrometer. The matrix correction method proposed by Lachance and Trail (1966) was applied. Volatile contents were determined as loss on ignition (L.O.I.) at 1000°C. The rare earth elements (REE) and some trace elements (Rb, Sr, Zr, Y, Nb, Hf, Ta, Th, U) were determined by inductively coupled plasma-mass spectrometry (ICP-MS) using a Thermo Series X-I spectrometer. All whole rock analyses were performed at the Department of Physics and Earth Sciences of the Ferrara University (Italy); results are shown in Supplementary Data (Table S1). The accuracy of the XRF and ICP-MS data were evaluated using results for international standard BE-N and BHVO-1 run as unknown. The detection limits for XRF and ICP-MS analyses were evaluated using results from several runs of twenty-nine international standards. Accuracy and detection limits are given in Supplementary Data (Table S2). For the discussion of the geochemical characteristics of the studied rocks, major element composition has been re-calculated on L.O.I.-free bases.

5. Whole-rock geochemistry

The geochemical features of volcanic rocks and dykes from the Remeshk-Mokhtarabad and Fannuj-Maskutan ophiolites will be described here using those elements that are virtually immobile during alteration and metamorphism, such as some incompatible trace elements (e.g., Ti, P, Zr, Y, Sc, Nb, Ta, Hf, Th), REE, and some transition metals (e.g., Ni, Co, Cr, V) (Pearce and Norry, 1979).

No systematic chemical differences can be observed among pillow lavas, massive lavas, sheeted dykes, and individual dykes. Likewise, no chemical differences can be observed between similar rock types from the Remeshk-Mokhtarabad and Fannuj-Maskutan units (Supplementary Data, Table S1). Therefore, we will describe volcanic rocks and dykes from both ophiolitic units collectively in this section. These rocks are mainly represented by basalts, while relatively fractionated rocks, such as basaltic andesites, andesites, and dacites are rare (Fig. 5). Mg# values in basalts (from either the volcanic sequence or sheeted dyke, or individual dykes) range from 70.5 to 49.5 (average is 58) suggesting that most of these

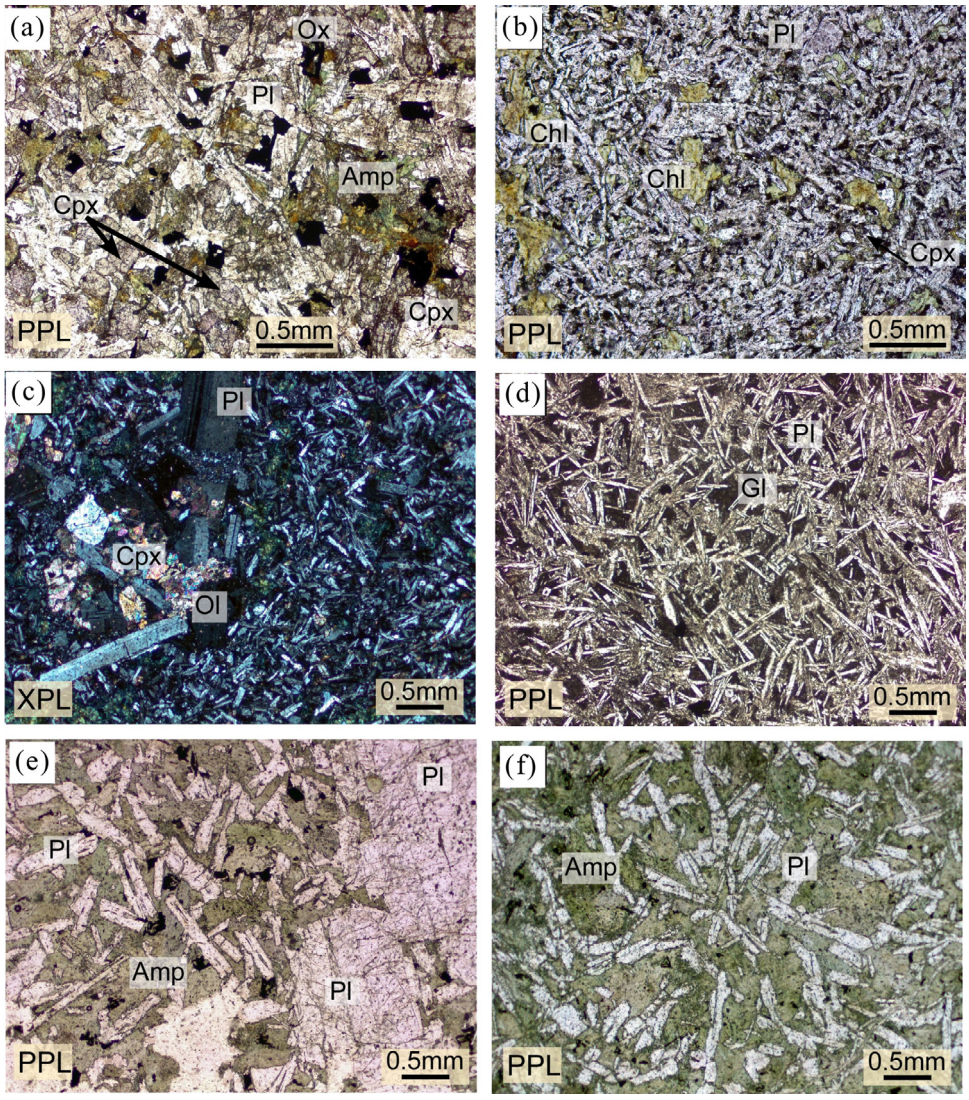

Fig. 4. Microphotos showing the main textures and mineral phase of the in the Remeshk-Mokhtarabad and Fannuj-Maskutan ophiolites. Abbreviations. PPL: plane polarized light; XPL: crossed polarized light; Amp: amphibole (tremolite); Chl: chlorite; Cpx: clinopyroxene; Ol: olivine; Ox: Fe–Ti-oxides; Pl: plagioclase. (a) Basalt MK175; (b) basalt MK209; (c) basaltic andesite MK205; (d) basalt MK192; (e) basalt MK2015; (f) basalt MK214.

basalts likely represent melts at a low to moderate degrees of magmatic fractionation, whereas relatively primitive basalts are subordinate. Basalts show variable contents of major elements and many trace elements (e.g., SiO_2, = 42.64–52.63 wt%, TiO_2 = 0.98–2.43 wt%, Al_2O_3 = 13.07–16.33 wt%, MgO = 4.12–11.66 wt%, Ga = 14–24 ppm, Zn = 26–134 ppm, *Sc* = 22–43 ppm, *V* = 191–370 ppm, Ni = 37–148 ppm, Cr = 119–530 ppm, see also Supplementary Data, Table S1). The variable contents of MgO, Cr, TiO_2, and V also suggest that these basalts represent melts ranging from rather primitive to moderately fractionated. A few basalts from both ophiolitic units show high contents of FeO_t (~13–15 wt%) and can be classified as ferrobasalts. Basaltic andesites and andesites are found in the Fannuj-Maskutan ophiolites, whereas dacites, which are the most fractionated rocks in our data set, are found in the Remeshk-Mokhtarabad unit. However, this cannot be considered as a distinguishing feature between these two ophiolitic units because of the very restricted number of intermediate to felsic rocks in our data set. Basaltic andesites and andesites show similar contents of major elements and many trace elements (e.g., SiO_2, = 54.64–59.90 wt%, TiO_2 = 0.95–1.58 wt%, Al_2O_3 = 13.52–14.14 wt%). These rocks are characterized by low MgO (4.93–7.57 wt%), Cr (2–61 ppm), Ni (20–30 ppm) coupled with relatively high P_2O_5 (0.20–0.74 wt%), Y (39.5–101 ppm), and Zr (326–504 ppm) (see Supplementary Data, Table S1). Compared to basaltic andesites and andesites, dacites show higher SiO_2 (67.76–69.78 wt%), Y (78.5–85.3 ppm), and Zr (558–620 ppm) contents coupled with very low MgO (1.12–2.38 wt%), TiO_2 (0.41–0.43 wt%), P_2O_5 (0.07–0.08 wt%), Cr (13–14 ppm). All the studied rocks show a sub-alkaline nature with Nb/Y ratios < 0.5 (Fig. 5). As shown above, the chemistry of these rocks points out for a general tholeiitic affinity. However, some incompatible elements (including REE), as well as many elemental ratios allow us to identify two distinct geochemical types (hereafter named as Type 1 and Type 2 rocks).

5.1. Type 1 volcanic rocks and dykes

Type 1 is represented only by two basalts from the Fannuj-Maskutan unit (one from the pillow lavas and one from the sheeted dykes) and one basaltic andesite (individual dyke) from the Remeshk-Mokhtarabad unit (see Supplementary Data, Table S1 and Fig. 2 for sample location). They display a sub-alkaline nature with very low Nb/Y ratio (0.09–0.10; Fig. 5). Basalts are

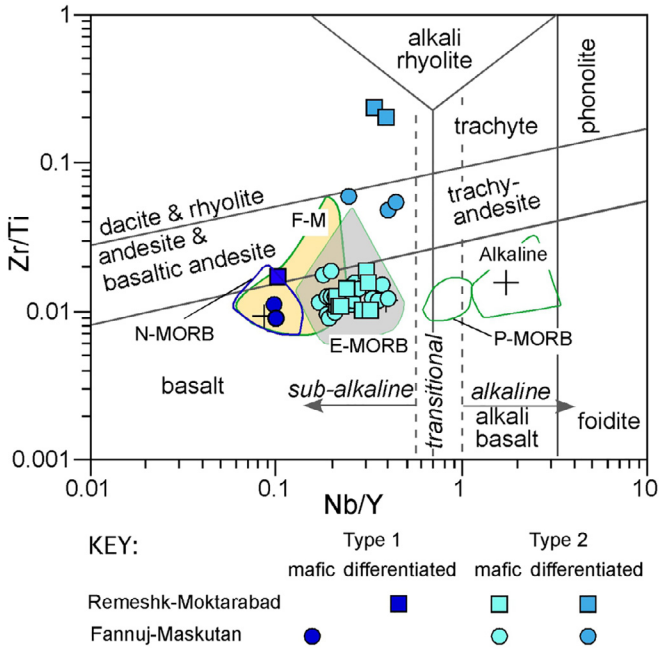

Fig. 5. Nb/Y vs. Zr/Ti discrimination diagram of Winchester and Floyd (1977) modified by Pearce (1996) for volcanic rocks and dykes from the Remeshk-Mokhtarabad and Fannuj-Maskutan ophiolites. The compositions of different rock types from various ophiolitic units of the North Makran domain, as well as literature data for the Fannuj-Maskutan (F-M) ophiolites (fields) are shown for comparison (data from Ghazi et al., 2004; Barbero et al., 2020b, 2021b; Sepidbar et al., 2020; Pandolfi et al., 2021; Saccani et al., 2022). Abbreviations, N-MORB: normal-type mid-ocean ridge basalt; E-MORB: enriched-type mid-ocean ridge basalt; P-MORB: plume-type mid-ocean ridge basalt.

characterized by generally low abundance of Y (19.4–30.3 ppm), Zr (55.6–99 ppm), Nb (1.86–2.82 ppm), Th (0.097–0.163 ppm), U (0.035–0.057 ppm), and Ta (0.094–0.167 ppm), as well as low Nb/Yb (0.87), Ta/Yb (0.04–0.05), and Th/Yb (0.05) ratios. Compared to basalts, the basaltic andesite shows relatively higher contents in incompatible elements and elemental ratios, which is consistent with a moderate degree of magmatic fractionation. In the N-MORB-normalized spider diagram (Fig. 6a), basalts show flat patterns, with a slightly negative anomaly in P. Contents of high-field strength elements (HFSE; e.g., Hf, Zr, Y) are low, ranging from ~0.7 to 1.2 times N-MORB composition (Sun and McDonough, 1989). The basaltic andesite shows a generally flat pattern with, however, a slight enrichment in Th, U, and Ta and a negative anomaly in Ti, which can be compatible with fractionation and removal of Fe–Ti phases. Chondrite-normalized REE patterns (Fig. 6b) are rather flat from MREE (middle REE) to HREE (heavy REE) in all samples. In basalts, LREE (light REE) shows depletion compared to MREE and HREE, as exemplified by the $(La/Yb)_N$ (0.50–0.75) and $(La/Sm)_N$ (0.48–0.72) ratios (Fig. 7). The basaltic andesite shows a flat pattern from LREE to HREE and a marked Eu positive anomaly (Fig. 6b), which is consistent with the significant abundance of plagioclase crystals in this rock. Incompatible elements and REE contents in basalts are either slightly lower or slightly higher than those of the typical N-MORB (Fig. 6a, b) with Yb_N values ranging from ~13 to 19 times chondrite abundance (Sun and McDonough, 1989). The incompatible and REE compositions of Type 1 basalts and basaltic andesite are well comparable with those of typical N-MORBs (Fig. 6a, b). In the discrimination diagram in Fig. 8, Type 1 basalts plot very close to the composition of N-MORBs (Saccani, 2015), whereas the basaltic andesite is shifted along the fractional crystallization trend. In general, Type 1 basalts show incompatible element composition and elemental ratios very similar to those of N-MORB rocks from various ophiolitic units of the North Makran (Figs. 5, 7, 8).

5.2. Type 2 volcanic rocks and dykes

Type 2 includes basalts, basaltic andesites, andesites, and dacites sampled from pillow and massive lava flows, as well as from the sheeted dyke complex and from individual dykes (see Supplementary Data, Table S1 and Fig. 2 for sample location and sample type). These rocks display a sub-alkaline nature with, however, Nb/Y ratios (0.16–0.38) that are visibly higher than those of Type 1 rocks (Fig. 5). These ratios overlap the Nb/Y values for E-MORBs from various ophiolitic units of the North Makran (Fig. 5). Likewise, though generally low, the abundances of Y (21.0–68.3 ppm), Zr (73.0–275 ppm), Nb (6.09–14.6 ppm), Th (0.420–1.600 ppm), U (0.072–0.379 ppm), and Ta (0.227–0.792 ppm) contents, as well as Nb/Yb (1.63–3.50), Ta/Yb (0.10–0.22), and Th/Yb (0.11–0.40) ratios in basalts are comparatively higher than those of Type 1 basalts. In the N-MORB-normalized incompatible elements spider diagram (Fig. 6c, e, g), Type 2 basalts show patterns slightly decreasing from Th to Yb with HFSE from 1 to 2 times N-MORB composition (Sun and McDonough, 1989). Chondrite-normalized REE patterns (Fig. 6d, F, h) are characterized by a slight enrichment in LREE compared to MREE and HREE, as exemplified by the $(La/Yb)_N$ (1.19–2.88) and $(La/Sm)_N$ (1.19–1.46) coupled with slight MREE/HREE enrichment (Sm_N/Yb_N = 1.16–2.01). These REE features are well summarized in Fig. 7, where all samples have LREE/HREE ratios >1. HREE contents are generally low with Yb_N values ranging from ~11 to 38 times chondrite abundance (Sun and McDonough, 1989). In addition, most Type 2 basalts show HREE contents slightly lower than those of the typical N-MORB (Yb_N = 17.9, Fig. 6d, f, h). The incompatible element and REE compositions of Type 2 basalts are well comparable with those of E-MORB (Fig. 6c-h). In fact, in the discrimination diagram in Fig. 8, Type 2 basalts plot around the compositions of E-MORBs (Saccani, 2015) and overlap the compositions of E-MORB rocks from various ophiolitic units of the North Makran. Accordingly, REE ratios plotted in Fig. 7 perfectly overlap those of E-MORB rocks from the North Makran ophiolitic units. In addition, it should be noted that in terms of incompatible element contents and ratios of Type 2 basalts are clearly different from those of P-MORB and alkaline basalts cropping out in other ophiolitic units of the North Makran (Figs. 5, 7, 8).

Type 2 basaltic andesites, andesites, and dacites show comparatively high contents of incompatible elements and REE, as shown in Fig. 6i, j. In the N-MORB-normalized incompatible elements spider diagram (Fig. 6i), Type 2 intermediate to felsic rocks show patterns whose trends are very similar to those of Type 2 basalts with, however, marked negative anomalies in P and Ti, which most likely reflect early crystallization and removal of apatite and Fe–Ti oxides. Chondrite-normalized REE patterns (Fig. 6j) are characterized by enrichment in LREE compared to MREE and HREE, as exemplified by the $(La/Yb)_N$ (2.72–3.96) and $(La/Sm)_N$ (1.70–2.20), as well as MREE/HREE enrichment (Sm_N/Yb_N = 1.54–2.05). All these rocks show marked Eu negative anomalies (Fig. 6j), which suggest early fractionation and removal of plagioclase. The relative enrichment in LREE with respect to MREE and HREE is slightly higher than that observed in basalts (Fig. 7a, b). In contrast, the relative enrichment in MREE with respect to HREE is comparable with that observed in basalts (Fig. 7b). The incompatible element and REE compositions of Type 2 intermediate to felsic rocks, as well as the relative LREE/MREE and LREE/HREE enrichment (Fig. 7a, b) are consistent with melts fractionated from E-MORB type primary melts. In fact, REE ratios (Fig. 7), and Th-Nb co-variation (Fig. 8) show that Type 2 basaltic andesites, andesites, and dacites plot along the fractional crystallization trend starting from E-MORB composition.

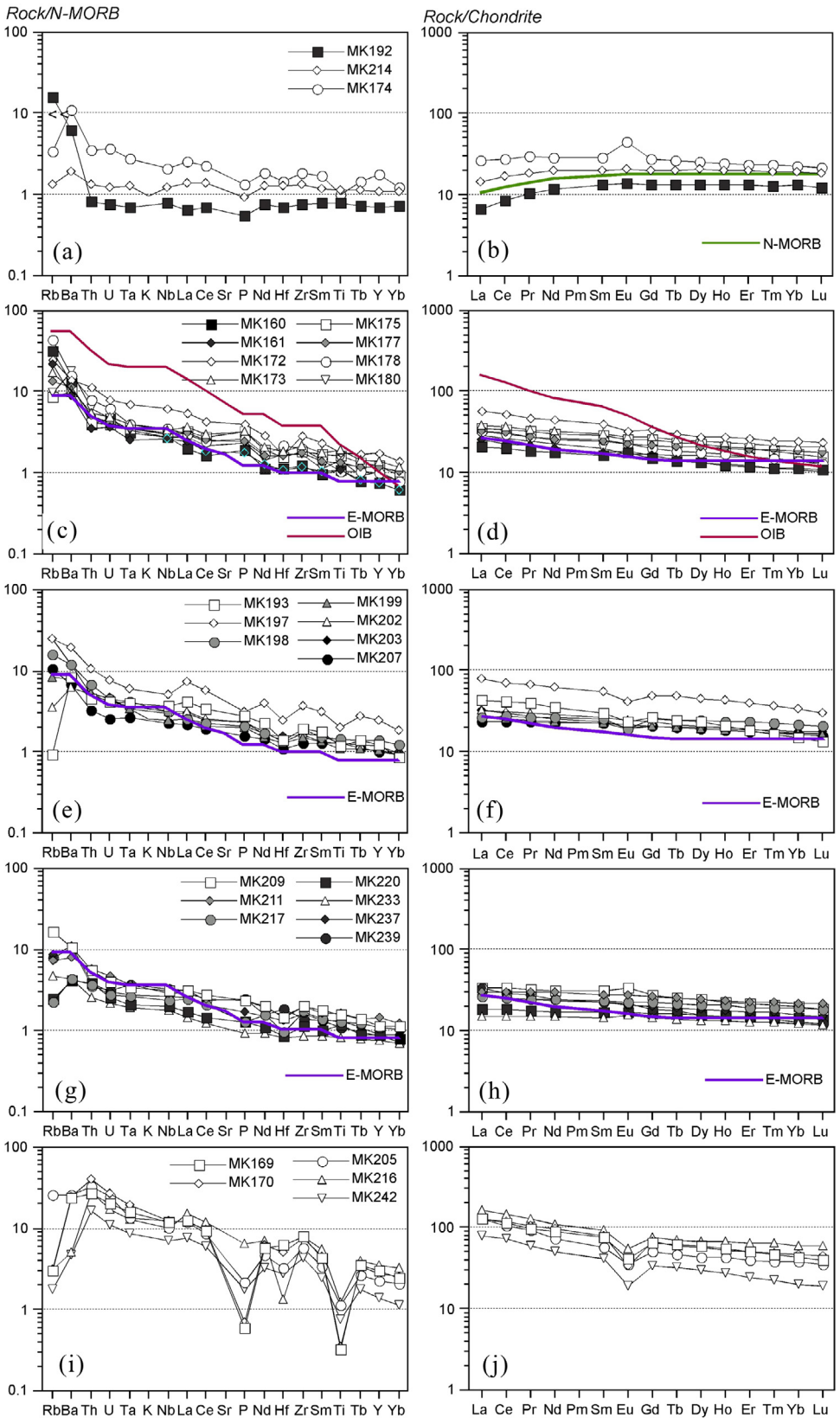

Fig. 6. N-MORB normalized incompatible element patterns (left column) and chondrite-normalized rare earth element patterns (right column) for volcanic rocks and dykes from the Fannuj-Maskutan ophiolites. Normalizing values are from Sun and McDonough (1989). Compositions of typical normal (N-MORB) and enriched (E-MORB) mid-ocean ridge basalts, and alkaline oceanic within-plate basalt (OIB) are from Sun and McDonough (1989).

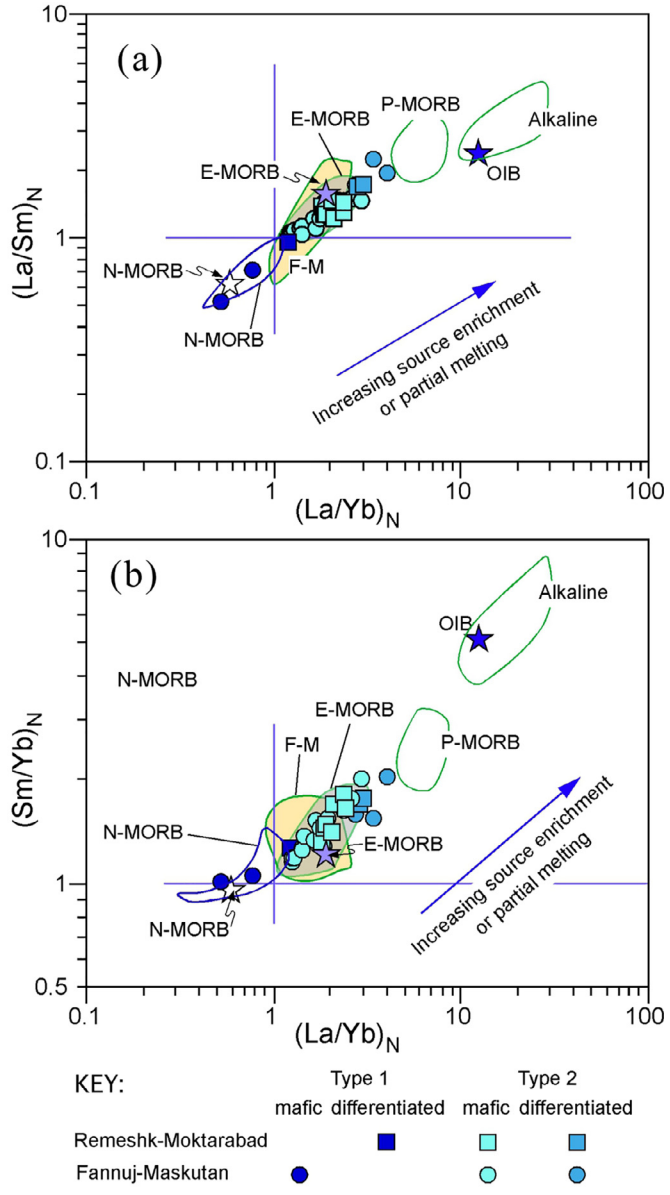

Fig. 7. Chondrite-normalized $(La/Sm)_N$ vs. $(La/Yb)_N$ (a) and $(Sm/Yb)_N$ vs. $(Sm/Yb)_N$ (b) diagrams for volcanic rocks and dykes from the Remeshk-Mokhtarabad and Fannuj-Maskutan ophiolites. Normalizing values, as well as the composition of typical N-MORB, E-MORB, and OIB (stars) are from Sun and McDonough (1989). Fields show the compositions of different rock types from various ophiolitic units of the North Makran domain, as well as literature data for the Fannuj-Maskutan (F-M) ophiolites (fields) are shown for comparison (data from Ghazi et al., 2004; Barbero et al., 2020b, 2021b; Sepidbar et al., 2020; Pandolfi et al., 2021; Saccani et al., 2022). Abbreviations, N-MORB: normal-type mid-ocean ridge basalt; E-MORB: enriched-type mid-ocean ridge basalt; P-MORB: plume-type mid-ocean ridge basalt; OIB: alkaline oceanic within-plate basalt.

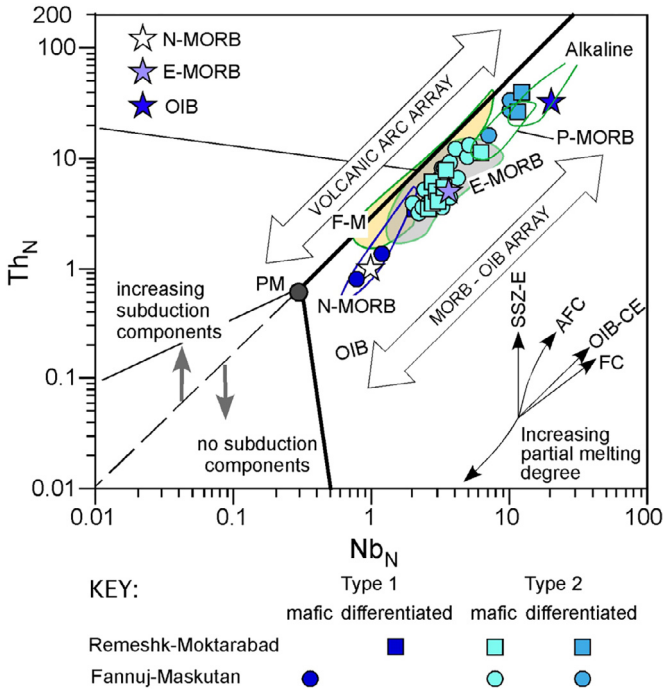

Fig. 8. N-MORB normalized Th vs. Nb discrimination diagram of Saccani (2015) for volcanic rocks and dykes from the Remeshk-Mokhtarabad and Fannuj-Maskutan ophiolites. Vectors indicate the trends of compositional variations due to the main petrogenetic processes. The compositions of different rock types from various ophiolitic units of the North Makran domain, as well as literature data for the Fannuj-Maskutan (F-M) ophiolites(fields) are shown for comparison (data from Ghazi et al., 2004; Barbero et al., 2020b, 2021b; Sepidbar et al., 2020; Pandolfi et al., 2021; Saccani et al., 2022). Abbreviations, N-MORB: normal-type mid-ocean ridge basalt; E-MORB: enriched-type mid-ocean ridge basalt; P-MORB: plume-type mid-ocean ridge basalt; OIB: alkaline oceanic within-plate basalt; AFC: assimilation-fractional crystallization; OIB-CE: ocean island-type (plume-type) component enrichment; FC: fractional crystallization. Normalizing values, as well as the composition of typical N-MORB, E-MORB, and OIB (stars) are from Sun and McDonough (1989).

6. Discussion

6.1. Petrogenesis of the basaltic melts

The aim of this discussion is to identify the possible mantle sources and melting conditions (e.g., depth and degree of partial melting) for the primary melts of the volcanic rocks and dykes from the Remeshk-Mokhtarabad and Fannuj-Maskutan ophiolites to provide robust constraints for the interpretation of their tectono-magmatic setting of formation. In fact, incompatible elements ratios of basaltic rocks, even in the presence of moderate amounts of fractional crystallization of olivine + plagioclase + clinopyroxene, is thought to be largely dependent on the composition and melting conditions of the mantle source rather than fractional crystallization processes (Allègre and Minster, 1978; Pearce and Norry, 1979).

Type 1 and Type 2 volcanic rocks and dykes described in Section 5 exhibit different trace elements contents (e.g., Zr, Y, Nb, Th) and REE patterns (Fig. 6), as well as different incompatible elements and REE ratios (e.g., Zr/Y, Ce/Y, Nb/Yb, La_N/Yb_N, Sm_N/Yb_N, Sm_N/Dy_N; Fig. 7) suggesting that these rocks were originated from partial melting of chemically distinct mantle sources and/or different melting conditions. The relatively less fractionated basalts (MgO > ~8 wt%) of Type 1 and Type 2 varieties show similar HREE contents (e.g., Yb_N = ~11 – ~18) but different LREE/HREE ratios (Fig. 7a) suggesting that their associated mantle sources most likely had experienced different enrichments in LREE, Zr, Nb, Th, Ta, and other incompatible elements. A first idea of the possible mantle sources associated with Type 1 and Type 2 rocks can be obtained from Fig. 9a, b. The Zr/Y-Zr/Nb covariation shows that the studied rocks plot along the mixing curve between N-MORB and OIB compositions with Type 1 basalts clustering around the composition of the typical N-MORB (Sun and McDonough, 1989). In contrast, Type 2 basalts plot between depleted (N-MORB) and enriched (E-MORB) end members, with a tendency to cluster toward the E-MORB composition (Fig. 9a). This diagram also shows that Type 1 basalts have Zr/Y and Zr/Nb ratios resembling those of N-MORB from the South Reykjanes Ridge in North Atlantic, whereas these elemental ratios for Type 2 basalts

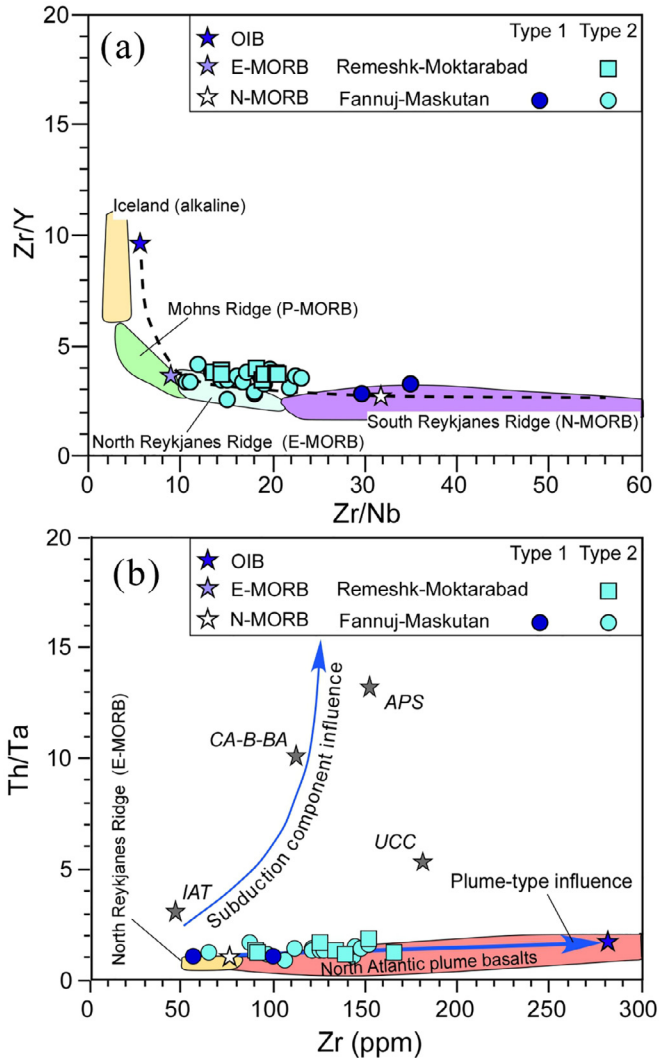

Fig. 9. (a) Zr/Y vs. Zr/Nb and (b) Th/Ta vs. Zr diagrams for mafic volcanic rocks and dykes from the Remeshk-Mokhtarabad and Fannuj-Maskutan ophiolites. The compositional variation for ocean-floor basalts erupted in the North Atlantic Ocean is shown for comparison (data from Thirlwall et al., 1984 and Hanan et al., 2000). The field North Atlantic plume basalts in panel b) includes E-MORBs from the North Reykjanes Ridge and P-MORBs from the Mohns Ridge. The dashed line in a) represents the mixing curve calculated using OIB and N-MORB end members (from Le Roex et al. 1983). Stars indicate the compositions of average pelitic sediments (APS), upper continental crust (UCC), average calc-alkaline basalts and basaltic andesites (CA-B-BA), average island arc tholeiitic basalts (IAT), normal-type mid-ocean ridge basalt (N-MORB), enriched-type mid-ocean ridge basalt (E-MORB), and alkaline ocean island basalt (OIB). P-MORB: plume-type mid-ocean ridge basalt. Data source: N-MORB, E-MORB, and OIB are from Sun and McDonough (1989); APS and UCC are from Taylor and McLennan (1985); IAT and CA-B-BA are calculated from 249 to 244 samples, respectively, of basaltic rocks from various ophiolitic complexes (see Table1 in Saccani, 2015 for references).

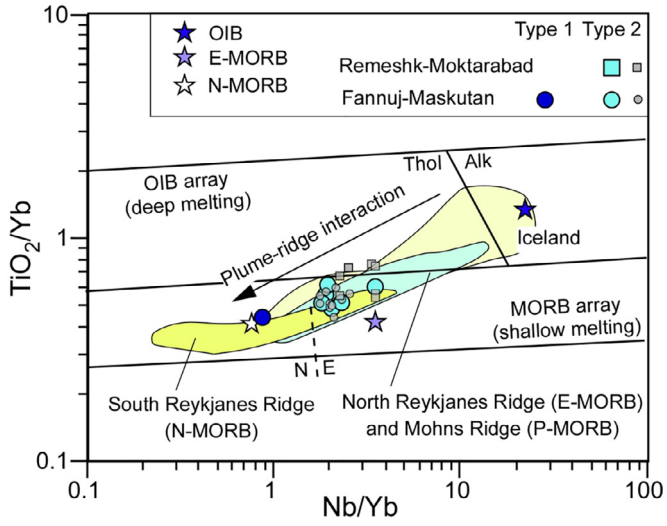

Fig. 10. TiO_2/Yb vs. Nb/Yb diagram (Pearce, 2008) for mafic volcanic rocks and dykes from the Remeshk-Mokhtarabad and Fannuj-Maskutan ophiolites. The compositional variation for ocean-floor basalts erupted in the North Atlantic Ocean is shown for comparison (data from Thirlwall et al., 1984 and Hanan et al., 2000). Abbreviations, N-MORB: normal-type mid-ocean ridge basalt; E-MORB: enriched-type mid-ocean ridge basalt; OIB: alkaline oceanic within-plate basalt. The relatively less fractionated basalts of each rock type are shown with large symbols, whereas other basaltic rocks are shown with small gray symbols.

are very similar to those of E-MORB from the North Reykjanes Ridge (Hanan et al., 2000). The geochemical variations in basalts from Iceland and the Reykjanes ridges have been attributed to mixing between the depleted MORB asthenosphere source and the enriched Iceland mantle plume (e.g., Thirlwall et al., 1994; Hanan et al., 2000, and references therein). The comparison with plume-influenced basalts from the North Atlantic suggests that Type 1 was most likely generated from a depleted MORB-type sub-oceanic mantle source, whereas Type 2 basalts are compatible with a genesis from depleted MORB-type mantle that was metasomatized by OIB-type (plume-type) chemical components. The Th-Nb co-variation (Fig. 8) further points out for a genesis of the studied rocks from partial melting of mantle sources that have been influenced by enriched OIB-type chemical components prior to melting without any contribution from subduction-related chemical components and/or continental crust contamination. However, some authors have suggested that LREE/HREE enrichment observed in many Fannuj-Maskutan ophiolitic basalts reflects chemical enrichment by fluid components derived from a subducting slab (Moslempour et al., 2015; Khalatbari-Jafari et al., 2016). Nonetheless, the Th/Ta-Zr co-variation shows that the influence of subduction components on the composition of both the Remeshk-Mokhtarabad and Fannuj-Maskutan basalts is absent or negligible (Fig. 9b). Rather, the Th/Ta-Zr co-variation of the studied basalts is similar to the geochemical variations observed from N-MORBs to plume-influenced E-MORBs from the Reykjanes Ridge.

The relatively high HREE contents (e.g., $Yb_N = \sim 11$ - ~ 18) in the most primitive basalts suggest no or little involvement of residual garnet in the mantle source. In fact, these rocks plot in the MORB array in the TiO_2/Yb vs. Nb/Yb diagram (Fig. 10a), suggesting that they derived from partial melting in the spinel-facies mantle (Pearce, 2008). Nonetheless, a small contribution from melts deriving from garnet-facies mantle cannot be straightforwardly excluded. The Nb/Yb ratios further suggest that Type 1 basalts were generated from a depleted N-MORB type mantle source without any influence of plume-type chemical components, whereas Type 2 basalts show Nb/Yb ratios higher than Type 1 rocks that indicate some contribution from plume–type components. Indeed, the TiO_2, Nb, and Yb compositions of Type 2 basalts are similar to that of plume-influenced basalts from the North Reykjanes Ridge (Fig. 10). Nonetheless, the relatively primitive Type 2 basalts in our data set show slightly different REE compositions at similar SiO_2 and MgO contents and Mg# values (Fig. 11). In particular, some of them show cross cutting REE patterns suggesting that they derived from slightly different mantle sources or that they experienced different extents of enrichments from plume-type components.

Given these assumptions, we performed semi-quantitative non-modal, batch partial melting models in order to define the possible mantle peridotite compositions and melting conditions that can reproduce the compositions of the relatively primitive basalts

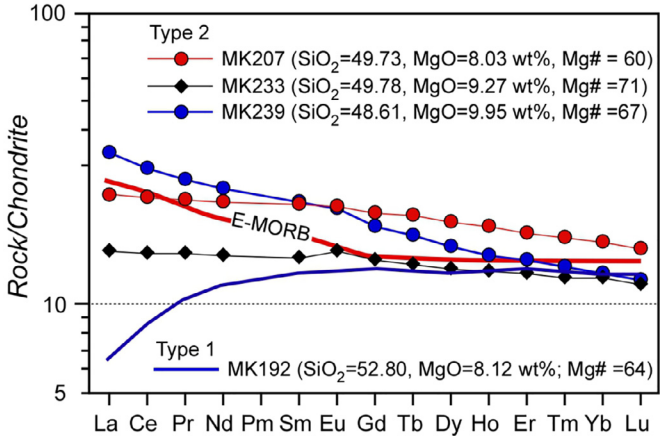

Fig. 11. Chondrite-normalized rare earth element patterns for the relatively most primitive Type 2 basalts from the Remeshk-Mokhtarabad and Fannuj-Maskutan ophiolites that were selected for petrogenetic models. Normalizing values are from Sun and McDonough (1989). Compositions of the relatively primitive Type 1 basalt and typical enriched (E-MORB) mid-ocean ridge basalts (Sun and McDonough, 1989) are also shown.

for each geochemical group. A quantitative definition of the various factors controlling partial melting (i.e., the composition of mantle sources, degrees and depths of partial melting, temperature, etc.) is very hard to be made when studying tectonically dismembered ophiolites. The non-modal, batch partial melting model was, therefore, used because the melt generated can be considered as a "single batch" of magma, which is not depending on a number of factors controlling the segregation of the melts from the mantle source. In contrast, other partial melting models require a rigorous definition of several factors (e.g., permeability threshold of the source, melt temperature, melt viscosity, etc.), which cannot be modeled in detail in our study. The magma chamber petrogenetic processes (e.g., fractional crystallization) cannot consistently be modeled because, due to the fragmented tectonic nature and different ages of formation (see Dolati, 2010) of the studied ophiolites, co-magmatic relationships between different samples within each magmatic group cannot be proved. Nonetheless, in our model we consider only relatively primitive basalts and we use elements whose contents are commonly assumed to largely depend on the composition of the mantle source and its degree of partial melting, rather than fractional crystallization (e.g., Allègre and Minster, 1978). Therefore, the effects of fractional crystallization can be assumed as negligible. Finally, given the semi-quantitative nature of our models, we used different models based on incompatible trace elements and trace element ratios (Nb/Y vs. Th; Zr vs. La), as well as REE in order to crosscheck the consistency of the results obtained from each model (Fig. 12). We have previously shown that the composition of Type 1 and Type 2 basalts from the Remeshk-Mokhtarabad and Fannuj-Maskutan ophiolites strongly points out for a genesis from partial melting of a sub-oceanic mantle source and sub-oceanic mantle sources that have experienced variable metasomatism from deep mantle OIB-type chemical components, respectively (Figs. 8, 9, 10). Therefore, in our models we chose as a possible mantle source for the Type 1 basalts the depleted MORB mantle (DMM) of Workman and Hart (2005). The possible mantle sources for Type 2 basalts are assumed as a DMM metasomatized to various extents of enrichment by an OIB-type chemical component, according to the models presented in Saccani et al., 2003; Bortolotti et al., 2018; Barbero et al., 2020b). In our models, we used the enriched mantle of Lustrino et al. (2002) as the metasomatizing chemical component. The modal compositions of the assumed mantle sources, their chemical composition, the melting proportions, and the REE

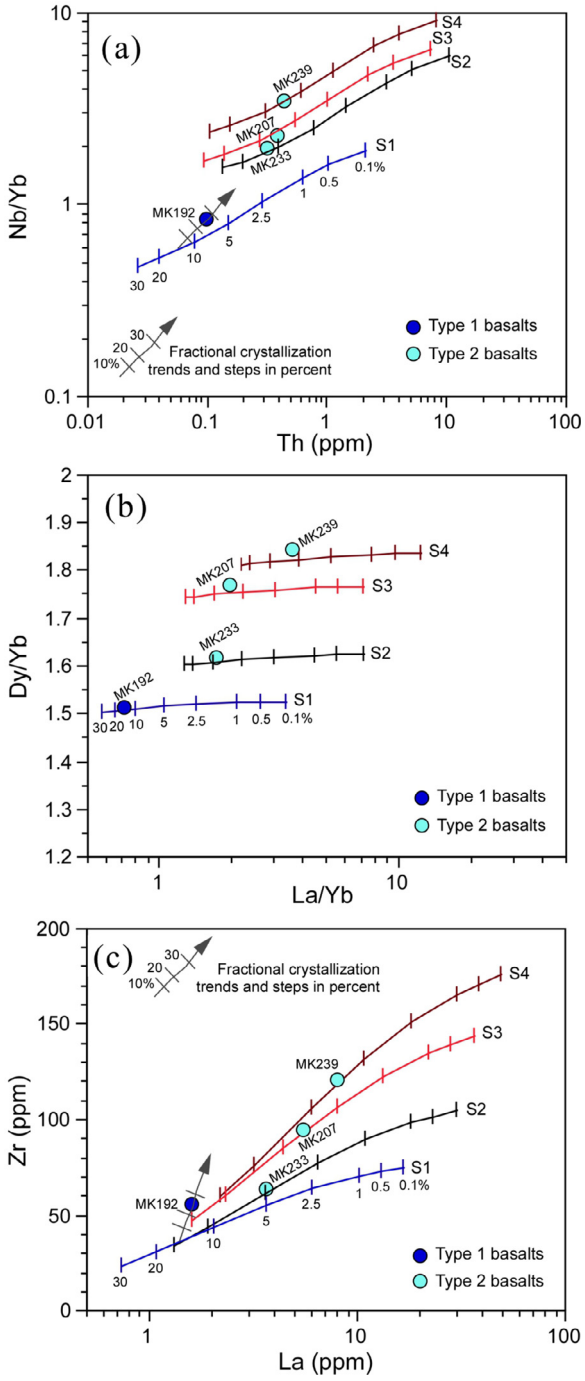

Fig. 12. (a) Nb/Yb vs. Th; (b) Dy/Yb vs. La/Yb; (c) Zr vs. La batch melting curves for different mantle sources. S1: depleted MORB mantle (DMM); S2, S3, S4: differently enriched MORB mantle sources. DMM composition is from Workman and Hart (2005), S2, S3, S4 represent theoretical mantle sources calculated by assuming different degrees of enrichment by an OIB-type chemical component (from Lustrino et al., 2002) of the DMM and primordial mantle (Sun and McDonough (1989). Melting curves are calculated for spinel-facies conditions following Saccani et al. (2003); Bortolotti et al. (2018); Barbero et al. (2020b). Input parameters (source modes, melting proportions, and partition coefficients, source compositions) for batch melting models are given in Supplementary Data (Table S3). Only the selected relatively primitive basalts of each rock type are shown.

and trace elements distribution coefficients used in the models are listed in Supplementary Data (Table S3).

6.1.1. Type 1 rocks

It should be noted that the most primitive Type 1 basalt MK192 we have in our data set likely represents a slightly fractionated

melt formed after about 20–25% fractional crystallization of olivine, plagioclase and clinopyroxene from a primitive tholeiitic melt. In fact, this sample has SiO_2 (52.80 wt%), MgO (8.12 wt%) and Mg# (64) slightly different from those of the typical primitive MORB (SiO_2 = 49.51 wt%; MgO = 9.74 wt%; Mg# = 70.6; Workman and Hart, 2005). Therefore, the fractional crystallization trends for the Nb/Y-Th and Zr-La compositions of this sample have been calculated to evaluate the composition of its parental primary melt. The Nb/Yb vs. Th petrogenetic model suggests that the compositions of Type 1 relatively primitive basalt MK192 can be explained by about 12–15% partial melting of the DMM in the spinel-facies mantle (Fig. 12a). Accordingly, the REE model, presented here as a plot of LREE/HREE (La/Yb) vs. MREE/HREE (Dy/Yb) ratios (Fig. 12b), clearly indicates that the REE composition of sample MK192 can be explained by 12–15% partial melting of the DMM source in the spinel-facies. The Zr vs. La model shows the same results as described above. In fact, the Zr vs. La co-variation of the relatively primitive Type1 basalt fits well with ~12–15% partial melting of the DMM source in the spinel facies.

6.1.2. Type 2 rocks

Once plotted in the models in Fig. 12, the most primitive Type 2 basalts we selected from our data set (see Fig. 11) show consistent results for the different models. Sample MK233 show the lowest LREE/HREE enrichment (La_N/Yb_N = 1.24) and the lowest absolute REE content within Type 2 rocks (Fig. 11). This basalt is compatible with ~10–12% partial melting of the theoretical source S2 in Fig. 12. This source corresponds to a mantle source slightly enriched in La, Th, Nb, and Zr with respect to a DMM source with, however, MREE and HREE similar to those of the Primitive Mantle (PM; Sun and McDonough, 1989).

Basalt MK207 shows low LREE/HREE enrichment (La_N/Yb_N = 1.24) coupled with the highest absolute MREE and HREE contents (Fig. 11). REE and Zr - La models indicate that this basalt is compatible with ~7–8% partial melting of the theoretical source S3 (Fig. 12b, c). The Nb/Yb - Th model generally confirms this conclusion (Fig. 12a). However, this basalt may represent a slightly fractionated liquid composition; therefore, a genesis of this basalt after small degrees of fractional crystallization starting from a primary melt generated, in turn, from ~10% to 12% partial melting of the theoretical source S2 should also be taken into account. Nonetheless, the REE composition of this sample cannot be explained by this hypothesis (Fig. 12b). The theoretical S3 source corresponds to a mantle source comparatively more enriched in La and Zr and less enriched in Th with respect to the S2 source, as well as with HREE contents similar to those of the DMM. It can, therefore, be postulated that source S3 may represent a sub-oceanic DMM variably enriched in LREE, Zr, Nb, and Th.

Basalt MK239 shows the highest LREE/HREE enrichment (La_N/Yb_N = 2.58) among the Type 2 primitive basalts. In fact, this sample shows the highest absolute LREE and the lowest HREE contents (Fig. 11). All the geochemical models suggest that this basalt is compatible with ~7–8% partial melting of the theoretical source S4 (Fig. 12). Compared to the S3 source, this source corresponds to a sub-oceanic mantle source more enriched in La, Zr, Nb, and Th. In fact, the composition of these elements is similar to that of the Primordial Mantle (Sun and McDonough, 1989), whereas MREE and HREE are analogous to those of the DMM (Workman and Hart, 2005). In conclusion, all Type 2 primary or near-primary basalts originated from sub-oceanic mantle sources enriched by plume-type geochemical components. Nonetheless, our petrological models show that the geochemical differences in Type 2 basalts from the Remeshk-Mokhtarabad and Fannuj-Maskutan ophiolites reflect different extents of mixing between depleted MORB asthenosphere and enriched mantle plume components, which characterized different oceanic sectors most likely in different times during the Early Cretaceous development of these ophiolites. Finally, we performed the models shown in Fig. 12 also using different melting conditions in terms of mantle source compositions, different degrees of partial melting, and different mantle depths (i.e., spinel- and garnet-facies conditions). However, all these calculations failed to reproduce the Nb-Th-Zr-REE composition of the primitive basalts of Type 2 and, therefore, are not shown.

6.2. Comparison with the North Makran ophiolitic and metaophiolitic units and tectono-magmatic significance

The geochemical data presented in this paper suggest that volcanic rocks and dykes of the Remeshk-Mokhtarabad and Fannuj-Maskutan ophiolites are represented by MORB-type rocks, which range in composition from normal- to enriched-type MORB. Accordingly, the petrogenetic models show that E-MORBs bear variable enrichment by plume-type chemical components (e.g., Th, Nb, LREE, Zr). Similar compositional variations in other ophiolitic and metaophiolitic units of the North Makran have been explained by many authors as related to variable plume-type influence (Ghazi et al., 2004; Saccani et al., 2018; Barbero et al., 2020a, 2020b, 2021a, 2021b; Esmaeili et al., 2020; Sepidbar et al., 2020; Barbero, 2021; Pandolfi et al., 2021). Therefore, regardless of the different metamorphic evolution recorded in the different units, a comparison between the rocks studied in this paper and mafic volcanic and metavolcanic rocks of other North Makran ophiolitic units can improve our knowledge on the nature and composition of the Makran Neo-Tethys during Mesozoic times.

6.2.1. A brief summary of geochemistry and petrogenesis of the North Makran ophiolites

The Band-e-Zeyarat sheeted dykes, and volcanic rocks are mainly represented by Late Jurassic-Early Cretaceous basalts showing either N-MORB or E-MORB affinities (Ghazi et al., 2004; Barbero et al., 2020b; Figs. 12a, b). According to Barbero et al. (2020b), N-MORBs formed by partial melting of a depleted sub-oceanic mantle peridotite in the spinel-facies, whereas E-MORBs were formed by partial melting of a depleted sub-oceanic mantle peridotite that was metasomatized by OIB-type (plume-type) components. These conclusions are also confirmed by Nd, Pb, and Sr isotopic data, which indicate that the Band-e-Zeyarat ophiolite was derived from more or less enriched MORB-like mantle sources (Ghazi et al., 2004). This ophiolite records, therefore, an Early Cretaceous plume-ridge interaction in the Makran Neo-Tethys (Ghazi et al., 2004; Barbero et al., 2020b).

The Deyader Metamorphic Complex includes tectonic slices of HP-LT blueschists derived from mafic protoliths (Hunziker, 2014; Hunziker et al., 2017). Saccani et al. (2022) have shown that metabasalts are represented by three geochemically distinct protoliths, including sub-alkaline basalts showing either N-MORB or E-MORB compositions and transitional basalts showing P-MORB composition (Fig. 13a). According to these authors, the Deyader basaltic protoliths derived from partial melting in the spinel-facies of a sub-oceanic mantle metasomatized to various extents by an OIB-type (plume-type) chemical component (Fig. 13b). In detail, N-MORBs originated from a near-pure DMM source, whereas E-MORBs, and P-MORBs derived from a DMM source slightly (E-type) or severely (P-type) enriched by plume-type components. Though the age of the basaltic protoliths of the Deyader blueschists is still unknown, Saccani et al. (2022) suggested that magmatic protoliths of the Deyader blueschists represent fragments of a Late Jurassic – Cretaceous oceanic basin that was strongly affected by mantle plume activity and different extents of plume-ridge interaction.

The Durkan Complex basalts and metabasalts display geochemistry ranging from transitional P-MORB to alkaline OIBs (Barbero et al., 2021b). These features are summarized in

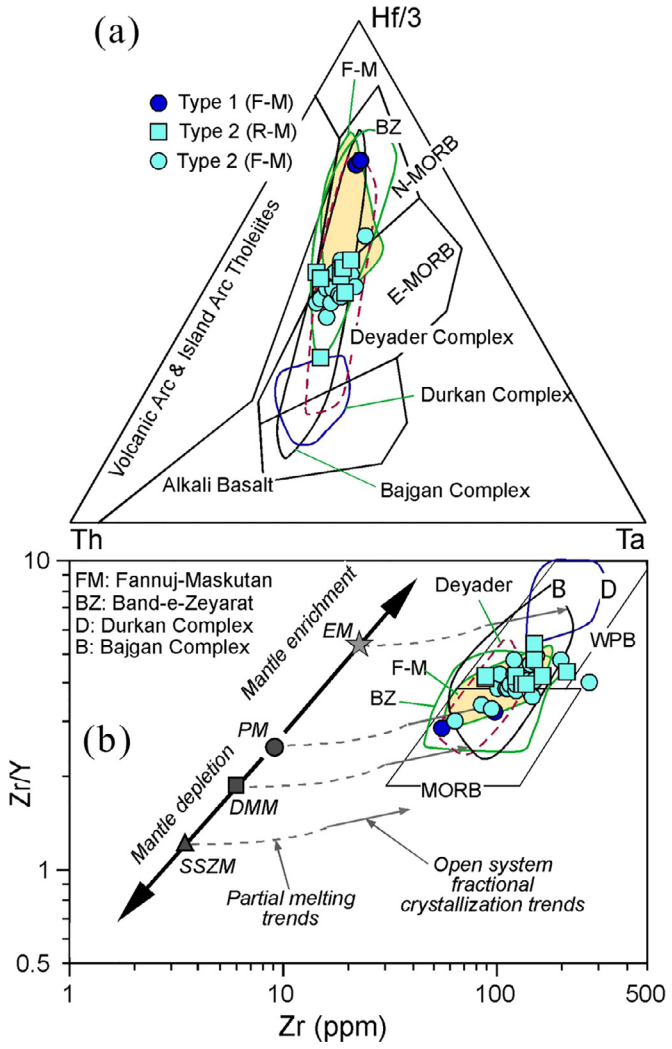

Fig. 13. Comparison between the composition of mafic volcanic rocks and dykes from the Remeshk-Mokhtarabad and Fannuj-Maskutan ophiolites studied in this paper, literature data for the Fannuj-Maskutan ophiolites (Ghazi et al., 2004; Moslempour et al., 2015; Khalatbari-Jafari et al., 2016; Sepidbar et al., 2020) and mafic volcanic and metavolcanic rocks and dykes from different ophiolitic units of the North Makran (Barbero et al., 2020b; 2021b; Pandolfi et al., 2021; Saccani et al., 2022). (a) Th-Ta-Hf/3 (Wood, 1980) discrimination diagram; (b) Zr/Y vs. Zr diagram (Pearce and Norry, 1979). Abbreviations, N-MORB: normal-type mid-ocean ridge basalt; E-MORB: enriched-type mid-ocean ridge basalt; WPB: within-plate alkaline basalt; PM: primordial mantle (Sun and McDonough, 1989); DMM: depleted MORB mantle (Workman and Hart, 2005); SSZM: depleted supra-subduction zone mantle (Photiades et al., 2003). Partial melting paths from PM, DMM, and SSZM are calculated based on Pearce and Norry (1979), Saccani et al. (2003), and Bortolotti et al. (2018).

Fig. 13a where these rocks plot across the boundary between E-MORB and alkaline basalts compositional fields. The Zr/Y vs. Zr co-variation shows that they plot in the within-plate oceanic field and are consistent with a genesis from enriched to very enriched mantle sources (Fig. 13b). Petrogenetic models shown by Barbero et al. (2021a, 2021b) indicate that the Durkan basaltic rocks were generated from the partial melting of a sub-oceanic mantle source that was metasomatized by OIB-type (plume-type) chemical components in a within-plate oceanic setting. These authors suggested that the chemical differences between P-MORBs and OIBs can be interpreted by different combinations of OIB-type enrichment, degree of partial melting, and depths of melting. Based on this evidence, the Durkan Complex has recently been interpreted as remnants of Late Cretaceous disrupted seamounts (Barbero et al., 2021a). These conclusions imply that the oceanic lithosphere onto which the Durkan seamounts were forming was characterized by an important mantle plume activity in the Late Cretaceous (Barbero et al., 2021b).

Recent studies have shown that the volcanic protoliths of the HP-LT metaophiolites of the Bajgan Complex are Late Jurassic to Early Cretaceous in age and consist of MORB type rocks ranging from depleted (N-MORB) to slightly enriched (E-MORB) compositions, as well as of alkaline OIBs (Barbero et al., 2021c; Pandolfi et al., 2021; Fig. 12a, b). Based on petrological and lithostratigraphic evidence, these authors suggested that the Bajgan Complex is represented by metaophiolites formed in different oceanic tectonic settings and from compositionally different mantle sources. In brief, N-MORB volcanic protoliths were generated in mid-ocean ridge settings from depleted mantle sources, the slightly enriched E-MORB volcanic protoliths were generated in plume-influenced mid-ocean ridge settings, and the enriched OIB-type protoliths were generated in within-plate seamounts associated with plume–type activity.

6.2.2. Tectono-magmatic significance of the Remeshk-Mokhtarabad and Fannuj-Maskutan ophiolitic basalts

The extrusive sequence of Fannuj-Maskutan ophiolites has been previously studied by several authors (Desmons and Beccaluva, 1983; Hunziker, 2014; Moslempour et al., 2015; Khalatbari-Jafari et al., 2016; Burg, 2018; Sepidbar et al., 2020). Selected data from these authors are shown in Fig. 13. However, no consensus exists about the petrogenetic mechanisms and tectonic setting of formation of these ophiolites. Desmons and Beccaluva (1983) related the genesis of the mafic lavas from these ophiolites to a mid-ocean ridge setting. Based on close similarities with mid-ocean ridge basalts, such as relatively high Ti, P, Y contents, coupled with Nb depletion, Moslempour et al. (2015) and Khalatbari-Jafari et al. (2016) suggested that they formed in a back-arc basin setting. Hunziker (2014) and Burg (2018) suggested that the Fannuj-Maskutan ophiolites, together with the Remeshk-Mokhtarabad unit, formed in a marginal basin, which originated, in turn, from the rifting and separation of the Bajgan continental ribbon from the Lut Block. In contrast, Sepidbar et al. (2020) suggested that these ophiolites show a petrogenetic evolution from early-stage island arc tholeiitic gabbros to later-stage E-MORB-like basalts (see Fig. 13a). Accordingly, the diagram in Fig. 13b (Pearce and Norry, 1979) shows that the Zr/Y-Zr co-variation of the Fannuj-Maskutan basalts is not compatible with a genesis from a depleted supra-subduction zone mantle. Rather, it is compatible with a genesis from a slightly enriched-type MORB mantle.

From Section 6.2.1 it is evident that the different ophiolitic and metaophiolitic units of the North Makran Domain represent fragments of both an oceanic crust that was forming in chemically composite mid-ocean ridge segments and oceanic within-plate seamounts. This oceanic crust developed from the Late Jurassic/Early Cretaceous to the Late Cretaceous and was largely characterized by mantle plume activity. As a general tendency, we can observe a magmatic evolution from depleted N-MORB and slightly enriched E-MORB compositions (e.g., Band-e-Zeyarat ophiolites; Ghazi et al., 2004; Barbero et al., 2020b) to comparatively more enriched P-MORB and alkaline OIB compositions (e.g., Durkan Complex; Barbero et al., 2021a, 2021b) from the Late Jurassic–Early Cretaceous to Late Cretaceous, suggesting an increasing influence of the mantle plume activity toward Late Cretaceous times (see also Barbero et al., 2021b). The Remeshk-Mokhtarabad and Fannuj-Maskutan volcanic rocks and dykes fit very well with the general context of formation of the North Makran ophiolites and metaophiolites. In fact, they are Early Cretaceous in age (Dolati, 2010) and show the same compositional varieties (i.e., N-MORB and E-MORB) observed in the coeval Band-e-Zeyarat ophiolites (Fig. 13a, b), as

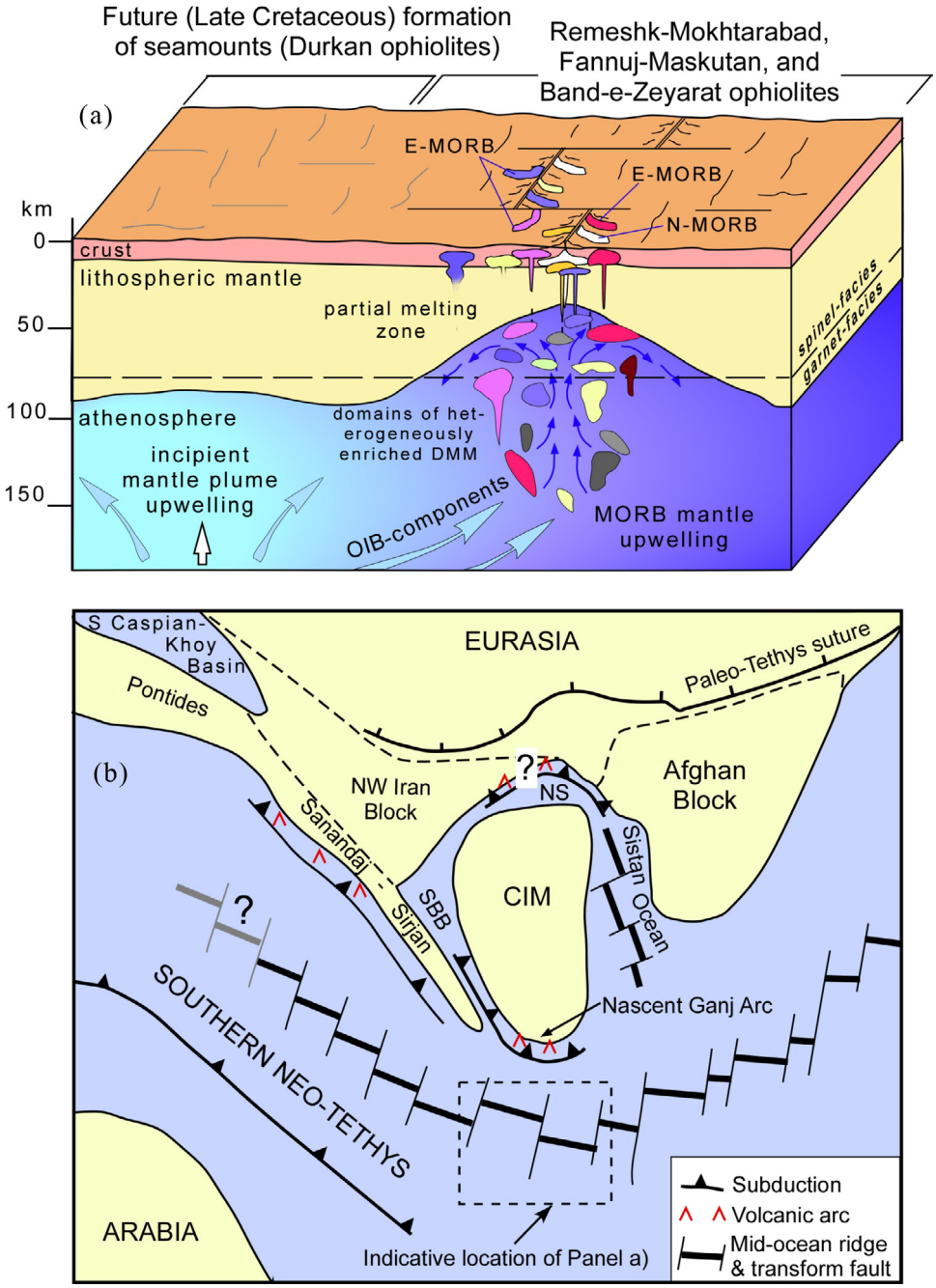

Fig. 14. (a) Schematic cartoon for explaining our preferred tectono-magmatic model for the petrogenesis of the Remeshk-Mokhtarabad and Fannuj-Maskutan ophiolites within the Makran sector of the Neo-Tethys at Early Cretaceous times. This model also applies to the entire North Makran ophiolitic and metaophiolitic units. At Early Cretaceous times, the incipient upwelling of deep mantle plume material (OIB-type material) variably contributed to the veining and enrichment of the originally depleted MORB mantle (DMM) with formation of blobs and domains of differently metasomatized mantle. N-MORBs derived from unveined depleted mantle. Chemically different E-MORBs derived from distinct enriched mantle domains characterized by variable OIB/DMM ratios. During Late Cretaceous times the upwelling of mantle plume material was sufficiently well developed to form seamounts with alkaline basalts and P-MORBs now recorded in the Durkan Complex. (b) Paleogeographic map of the Neo-Tethys Ocean and surrounding continental domains in the Middle East area in the upper Early Cretaceous (modified from Barrier et al., 2018 and based on data from Esmaeili et al., 2020; Pirnia et al., 2020; Barbero et al., 2021a, 2021b; Pandolfi et al., 2021; Moghadam et al., 2022; Saccani et al., 2022). Abbreviations in Panel 14b, CIM: Central Iran Microcontinent; NS: Nain-Sabzevar Ocean; SBB: Share Babak-Baft Ocean. Question marks indicate that no general consensus exists about the tectonic setting in some areas.

well as similar petrogenetic processes (see Barbero et al., 2020b). In addition, the Remeshk-Mokhtarabad and Fannuj-Maskutan ophiolites are lacking significantly enriched P-MORBs and alkaline basalts, which are instead common in the Late Cretaceous Durkan Complex (Barbero et al., 2021a; 2021b).

This allows us to suggest that the Remeshk-Mokhtarabad and Fannuj-Maskutan ophiolites, similar to all the other ophiolitic and metaophiolitic units of the North Makran Domain, represent fragments of a unique Late Jurassic–Cretaceous oceanic basin that was strongly affected by mantle plume activity and plume-ridge interaction. It is interesting to note that the mantle plume activity was a widespread and important phenomenon in the entire Tethyan realm (e.g., Laws and Wilson 1997; Al-Riyami and Robertson 2002; Lapierre et al., 2004; Sayit 2013). In particular, mantle plume activity most likely affected the Middle East Neo-Tethys at a regional scale since Late Jurassic times, as recorded in the northern

sector of Sanandaj-Sirjan Zone (Azizi et al., 2018; H. 2020) and in the Caucasus (Rolland et al., 2010; 2020). A possible tectono-magmatic scenario in which the Early Cretaceous Remeshk-Mokhtarabad and Fannuj-Maskutan ophiolites, along with the coeval Band-e-Zeyarat ophiolites were generated is shown in Fig. 14a, whereas a schematic paleogeographic map of the Middle East sector of the Neo-Tethys during Cretaceous times is shown in Fig. 14b. This model takes into account several characteristics of these ophiolites, including: (1) the mixing relationships between enriched and depleted mantle; (2) the contemporaneous eruption of enriched and depleted magmas; (3) the regional-scale tendency of variation from depleted and little enriched products to very enriched products from Early to Late Cretaceous; (4) the variation in incompatible elements and REE observed within Type 2 E-MORBs; (5) the lack of apparent geochemical variations in time.

The model we propose implies that during Early Cretaceous the incipient uprising of mantle plume materials (OIB-type components) interacted with the upwelling depleted MORB mantle by variably metasomatizing portions of the originally depleted mantle. The regional-scale broad variation from depleted to progressively more enriched products from the Early to Late Cretaceous allows us to speculate that the enrichment of the depleted mantle by plume-type components during the Early Cretaceous occurred mainly with depth, rather than laterally (Fig. 14a). The metasomatism by OIB-type components resulted in the formation of a heterogeneous mantle with domains characterized by different enrichment in incompatible elements and REE (Fig. 14a). Partial melting of mantle regions with negligible enrichment in OIB-type components resulted in the production of N-MORBs. In contrast, chemically different E-MORBs are the result of partial melting of the mantle bearing different extents of OIB-type contribution. In the Remeshk-Mokhtarabad and Fannuj-Maskutan ophiolites, E-MORBs are largely predominant in volume compared to N-MORB suggesting that the mantle sources were predominantly characterized by metasomatized material. Nonetheless, though volumetrically subordinate, the eruption of N-MORBs was coeval with the eruption of E-MORBs further supporting the hypothesis of a strongly heterogeneous mantle. In fact, N-MORB sample MK214 represents a dyke in a coherent sheeted dyke outcrop (Fannuj-Maskutan unit) that was collected beside other dykes (samples MK215, MK216, and MK217) showing E-MORB chemistry (see Fig. 3c, d). In addition, sample MK216 is represented by a differentiated andesite. The occurrence of very different rock types (in terms of both chemical affinity and fractionation degrees) within a few metres (see Fig. 3c, d) in the same coherent dyke complex further supports the idea that this sheeted dyke complex was formed by intrusions of melts formed by tapping different portions of a heterogeneous mantle and/or different portions of magma chambers at different fractionation stages (see the general model in Fig. 14a). The progressive uprising of mantle plume material resulted in increasing plume-ridge interaction with formation of Late Cretaceous P-MORBs and alkaline basalts in either plume-proximal mid-ocean ridges or seamounts (Barbero et al., 2021a; 2021b; Saccani et al., 2022).

7. Conclusions

The Remeshk-Mokhtarabad and Fannuj-Maskutan ophiolites represent two major tectonic elements of the North Makran Domain and consist of tectonic slices of upper oceanic lithosphere. Compared to upper mantle and intrusive rocks, the volcanic rocks and dykes are subordinate in volume. The geochemical and petrogenetic study on volcanic rocks and dykes, as well as a geochemical comparison with similar rocks from other North Makran ophiolitic and metaophiolitic units allows the following conclusion to be drawn:

1) Volcanic rocks and dykes of the Remeshk-Mokhtarabad and Fannuj-Maskutan ophiolites mainly consist of basalts and subordinate basaltic andesites, andesites and dacites. No chemical distinction can be seen between these two ophiolitic units. Based on whole rock geochemical features, basaltic rocks are sub-alkaline and show both N-MORB (Type 1) and E-MORB (Type 2) compositions. Nonetheless, Type 1 rocks are very rare in both ophiolitic units, whereas Type 2 rocks are predominant.
2) Petrogenetic models based on several incompatible elements, such as REE, Th, Nb, and Zr, indicate that the relatively primitive basalts derived from partial melting in the spinel-facies of a sub-oceanic mantle metasomatized to various extents by OIB-type (plume-type) chemical components. In detail, Type 1N-MORBs derived from partial melting of mantle regions with negligible enrichment in OIB-type components, whereas Type 2 E-MORBs derived from different degrees of partial melting of a DMM source variably enriched by OIB-type components.
3) Petrological models show that little but appreciable differences in the chemistry of Type 2 E-MORBs can be related to different extents of enrichment of the depleted mantle by OIB-components, which resulted in the formation of a strongly heterogeneous sub-oceanic mantle. This hypothesis is further supported by the close association in both space and time of N- and E-MORBs.
4) Relatively primitive basalts from the Remeshk-Mokhtarabad and Fannuj-Maskutan ophiolites show the same compositions and petrogenetic mechanisms observed in basaltic rocks from other Early Cretaceous ophiolitic units from the North Makran Domain (e.g., the Band-e-Zeyarat unit). In contrast, they show some differences with the Late Cretaceous ophiolitic and metaophiolitic units (e.g., Durkan, Bajgan, and Deyader units).
5) Based on a comparison with the North Makran ophiolitic and metaophiolitic units, as well as regional evidence, we propose that the Remeshk-Mokhtarabad and Fannuj-Maskutan ophiolites represent a fragment of a unique Late Jurassic – Cretaceous oceanic basin in which all the ophiolitic and metaophiolitic units of the North Makran Domain were formed. This basin was strongly affected by mantle plume activity and different extents of plume-ridge interaction.

Declaration of Competing Interest

The authors declare that they have no known competing financial interests or personal relationships that could have appeared to influence the work reported in this paper.

CRediT authorship contribution statement

Emilio Saccani: Conceptualization, Investigation, Writing – original draft, Writing – review & editing, Project administration, Funding acquisition. **Morteza Delavari:** Conceptualization, Investigation, Writing – review & editing. **Asghar Dolati:** Conceptualization, Investigation, Writing – review & editing. **Luca Pandolfi:** Conceptualization, Investigation, Writing – review & editing, Project administration. **Edoardo Barbero:** Conceptualization, Investigation, Writing – review & editing. **Valentina Brombin:** Conceptualization, Investigation, Writing – review & editing. **Michele Marroni:** Conceptualization, Investigation, Writing – review & editing, Project administration, Funding acquisition.

Acknowledgement

The research has been funded by: Darius Project (Head M. Marroni), PRA project of the Pisa University (Head S. Rocchi), IGG-CNR, FAR-2020-2021 Projects of the Ferrara University (Head E. Saccani).

Mr. Ahmad Behboodi is sincerely thanked for his appreciated assistance in organizing field work. Constructive and thorough reviews for the Journal by two anonymous reviewers have helped us improve the science and organization presented in the paper. We are grateful to the Guest Editor for his insightful comments and editorial help.

Supplementary materials

Supplementary material associated with this article can be found, in the online version, at doi:10.1016/j.geogeo.2022.100140.

References

Allahyari, K., Saccani, E., Rahimzadeh, B., Zeda, O., 2014. Mineral chemistry and petrology of highly magnesian ultramafic cumulates from the Sarve-Abad (Sawlava) ophiolites (Kurdistan, NW Iran): new evidence for boninitic magmatism in intra-oceanic fore-arc setting in the Neo-Tethys between Arabia and Iran. J. Asian Earth Sci. 79, 312–328. doi:10.1016/j.jseaes.2013.10.005.

Allègre, C.J., Minster, J.F., 1978. Quantitative models of trace element behavior in magmatic processes. Earth Planet Sci. Lett. 38, 1–25. doi:10.1016/0012-821X(78)90123-1.

Azizi, H., Lucci, F., Stern, R.J., Hasannejad, S., Asahara, Y., 2018. The Late Jurassic Panjeh submarine volcano in the northern Sanandaj-Sirjan Zone, northwest Iran: mantle plume or active margin? Lithos 308–309, 364–380. doi:10.1016/j.lithos.2018.03.019.

Al-Riyami, K., Robertson, A., 2002. Mesozoic sedimentary and magmatic evolution of the Arabian continental margin, northern Syria: evidence from the Baer-Bassit Melange. Geol. Mag. 139, 395–420.

Azizi, H., Nouri, F., Stern, R.J., Azizi, M., Lucci, F., Asahara, Y., Zarinkoub, M.H., Chung, S.L., 2020. New evidence for Jurassic continental rifting in the northern Sanandaj Sirjan Zone, western Iran: the Ghalaylan seamount, southwest Ghorveh. Int. Geol. Rev. 62, 1635–1657. doi:10.1080/00206814.2018.1535913.

Barbero, E., 2021. Geological and Petrological Investigation of the Western North Makran Ophiolites (SE Iran): New Constraints For the Late Jurassic-Cretaceous Tectono-Magmatic and Geodynamic Evolution of the Neo-Tethys Ocean. University of Ferrara, Italy, p. 324.

Barbero, E., Delavari, M., Dolati, A., Saccani, E., Marroni, M., Catanzariti, R., Pandolfi, L., 2020a. The Ganj Complex reinterpreted as a Late Cretaceous volcanic arc: implications for the geodynamic evolution of the North Makran domain (southeast Iran). J. Asian Earth Sci. 195, 104306. doi:10.1016/j.jseaes.2020.104306.

Barbero, E., Delavari, M., Dolati, A., Vahedi, L., Langone, A., Marroni, M., Pandolfi, L., Zaccarini, F., Saccani, E., 2020b. Early cretaceous plume–ridge interaction recorded in the band-e-zeyarat ophiolite (North Makran, Iran): new constraints from petrological, mineral chemistry, and geochronological data. Minerals 10, 1100. doi:10.3390/min10121100.

Barbero, E., Pandolfi, L., Delavari, M., Dolati, A., Saccani, E., Catanzariti, R., Lucani, V., Chiari, M., Marroni, M., 2021a. The western Durkan complex (Makran Accretionary Prism, SE Iran): a late cretaceous tectonically disrupted seamounts chain and its role in controlling deformation style. Geosci. Front. 12, 101106. doi:10.1016/j.gsf.2020.12.001.

Barbero, E., Zaccarini, F., Delavari, M., Dolati, A., Saccani, E., Marroni, M., Pandolfi, L., 2021b. New evidence for Late Cretaceous plume-related seamounts in the Middle East sector of the Neo-Tethys: constraints from geochemistry, petrology, and mineral chemistry of the magmatic rocks from the western Durkan Complex (Makran Accretionary Prism, SE Iran). Lithos 396–397, 106228. doi:10.1016/j.lithos.2021.106228.

Barbero, E., Delavari, M., Dolati, A., Langone, A., Pandolfi, L., Marroni, M., Saccani, E., 2021c. New geochemical and age data on the Bajgan Complex (Makran Accretionary Prism, SE Iran): implications for the redefinition of its tectonic setting of formation from a Paleozoic continental basement to a Cretaceous oceanic domain. In: Mediterranean Geosciences Union Annual Meeting (MedGU-21), Istanbul, November 25-28, 2021, Conference Proceedings, SpringerLink Digital Library, p. 4.

Barrier, E., Vrielynck, B., Brouillet, J.F., Brunet, M.F., 2018. Paleotectonic Reconstruction of the Central Tethyan Realm. Tectono-Sedimentary-Palinspastic maps from Late Permian to Pliocene. Atlas of 20 maps (scale: 1:15.000.000). CCGM/CGMW, Paris, http://www.ccgm.org.

Beccaluva, L., Di Girolamo, P., Macciotta, G., Morra, V., 1983. Magma affinities and fractionation trends in ophiolites. Ofioliti 8, 307–324.

Bortolotti, V., Chiari, M., Goncuoglu, M.C., Principi, G., Saccani, E., Tekin, U.K., Tassinari, R., 2018. The Jurassic–early cretaceous basalt–chert association in the ophiolites of the Ankara Mélange, east of Ankara, Turkey: age and geochemistry. Geol. Mag. 155, 451–478. doi:10.1017/S0016756817000401.

Bröcker, M., Omrani, H., Berndt, J., Moslempour, M.E., 2021. Unravelling metamorphic ages of suture zone rocks from the Sabzevar and Makran areas (Iran): robust age constraints for the larger Arabia–Eurasian collision zone. J. Metamorph. Geol. 39, 1099–1129. doi:10.1111/jmg.12603.

Burg, J.-P., 2018. Geology of the onshore Makran accretionary wedge: synthesis and tectonic interpretation. Earth-Sci. Rev. 185, 1210–1231. doi:10.1016/j.earscirev.2018.09.011.

Burg, J.-P., Bernoulli, D., Smit, J., Dolati, A., Bahroudi, A., 2008. A giant catastrophic mud-and-debris flow in the Miocene Makran. Terra Nova 20, 188–193. doi:10.1111/j.1365-3121.2008.00804.x.

Burg, J.-P., Dolati, A., Bernoulli, D., Smit, J., 2013. Structural style of the Makran tertiary accretionary complex in SE Iran, in: al Hosani, K., Roure, F., Ellison, R., Lokier, S. (Eds.), lithosphere dynamics and sedimentary basins: the Arabian plate and analogues. Front. Earth Sci. 5, 239–259. doi:10.1007/978-3-642-30609-9_12.

Delavari, M., Dolati, A., Marroni, M., Pandolfi, L., Saccani, E., 2016. Association of MORB and SSZ ophiolites along the shear zone between Coloured Mélange and Bajgan Complexes (North Maran, Iran): evidence from the Sorkhband area. Ofioliti 41, 21–34. doi:10.4454/ofioliti.v41i1.451.

Delaloye, M., Desmons, J., 1980. Ophiolites and mélange terranes in Iran: a geochronological study and its paleotectonic implications. Tectonophysics 68, 83–111. doi:10.1016/0040-1951(80)90009-8.

Dercourt, J., Zonenshian, L.P., Ricou, L.E., Kazmin, V.G., LePichon, X., Knipper, A.L., Grandjacquet, C., Sbortshikov, M., Geyssant, J., Lepvrier, C., Pechersky, D.H., Boulin, J., Sibuet, J.C., Savostin, L.A., Sorokhtin, O., Westphal, M., Bazhenov, M.L., Lauer, J.P., Biju-Duval, B., 1986. Geological evolution of the Tethys belt from the Atlantic to the Pamir since the lias. Tectonophysics 123, 241–315. doi:10.1016/0040-1951(86)90199-X.

Desmons, J., Beccaluva, L., 1983. Mid-Ocean ridge and island-arc affinities in ophiolites from Iran: palaeographic implications. Chem. Geol. 39, 39–63. doi:10.1016/0009-2541(83)90071-2.

Dilek, Y., Furnes, H., 2011. Ophiolite genesis and global tectonics: geochemical and tectonic fingerprinting of ancient oceanic lithosphere. Geol. Soc. Am. Bull. 123, 387–411. doi:10.1130/B30446.1.

Dolati, A., 2010. Stratigraphy, Structure Geology and Low-temperature Thermochronology Across the Makran Accretionary Wedge in Iran. ETH, Zurich, p. 165.

Dolati, A., Burg, J.-P., 2013. Preliminary fault analysis and paleostress evolution in the Makran Fold-and-Thrust Belt in Iran. In: Al Hosani, K., Roure, F., Ellison, R., Lokier, S. (Eds.), Lithosphere Dynamics and Sedimentary Basins: The Arabian Plate and Analogues. Frontiers in Earth Sciences. Springer, Heidelberg, pp. 261–277. doi:10.1007/978-3-642-30609-9_13.

Dorani, M., Arvin, M., Oberhänsli, R., Dargahi, S., 2017. P-T evolution of metapelites from the Bajgan complex in the Makran accretionary prism, south eastern Iran. Geochemistry 77, 459–475. doi:10.1016/j.chemer.2017.07.004.

Eftekhar-Nezhad, J., Arshadi, S., Mahdavi, M.A., Morgan, K.H., McCall, G.J.H., Huber, H., 1979. Fannuj quadrangle map 1:250000. Ministry of mines and metal, Geological Survey of Iran, Tehran.

Esmaeili, R., Xiao, W., Ebrahimi, M., Zhang, J.E., Zhang, Z., El-Rahman, Y.A., Han, C., Wan, B., Ao, S., Song, D., Shahabi, S., Aouizerat, A., 2020. Makran ophiolitic basalts (SE Iran) record Late Cretaceous Neotethys plume-ridge interaction. Int. Geol. Rev. 62, 1677–1697. doi:10.1080/00206814.2019.1658232.

Esmaeili, R., Ao, S., Shafaii Moghadam, H., Zhang, Z., Griffin, W.L., Ebrahimi, M., Xiao, W., Wan, B., Bhandari, S., 2021. Amphibolites from Makran accretionary complex record Permian-Triassic Neo-Tethyan evolution. Int. Geol. Rev. doi:10.1080/00206814.2021.1946663.

Ghazi, A.M., Hassanipak, A.A., Mahoney, J.J., Duncon, R.A., 2004. Geochemical characteristics, 40Ar-39Ar ages and original tectonic setting of the Band-e-Zeyarat/Dar Anar ophiolite, Makran accretionary Prism, S.E. Iran. Tectonophysics 193, 175–196. doi:10.1016/j.tecto.2004.07.035.

Glennie, K.W., Hughes Clarke, M.W., Boeuf, M.G.A., Pilaar, W.F.H., Reinhardt, B.M., 1990. Inter-relationship of Makran-Oman Mountains belts of convergence, in: robertson, A.H.F., Searle, M.P., Ries, A.C. (Eds.), The Geology and Tectonics of the Oman Region. Geol. Soc. Spec. Publ. Lond. 49, 773–786. doi:10.1144/GSL.SP.1992.049.01.47.

Hanan, B.B., Blichert-Toft, J., Kingsley, R., Schilling, J.-G., 2000. Depleted Iceland mantle plume geochemical signature: artifact of multicomponent mixing? Geochem. Geophys. 1 (4). doi:10.1029/1999GC000009.

Hunziker, D., 2014. Magmatic and metamorphic history of the North Makran ophiolites and blueschists (SE Iran). Influence of Fe3+/Fe2+ Ratios in Blueschist Facies Minerals on Geothermobarometric Calculations. Eidgenössische Technische Hochschule ETH Zürich Doctoral dissertation.

Hunziker, D., Burg, J.-P., Bouilhol, P., von Quadt, A., 2015. Jurassic rifting at the Eurasian Tethys margin: geochemical and geochronological constraints from granitoids of North Makran, southeastern Iran. Tectonics 34, 571–593. doi:10.1002/2014TC003768.

Hunziker, D., Burg, J.-P., Moulas, E., Reusser, E., Omrani, J., 2017. Formation and preservation of fresh lawsonite: geothermobarometry of the North Makran Blueschists, southeast Iran. J. Metamorph. Geol. 35, 871–895. doi:10.1111/jmg.12259.

Khalatbari-Jafari, M., Babaie, H.A., Moslempour, M.E., 2016. Mid-ocean-ridge to suprasubduction geochemical transition in the hypabyssal and extrusive sequences of major Upper Cretaceous ophiolites of Iran, in: sorkhabi, R. (Ed.), Tectonic Evolution, Collision, and Seismicity of Southwest Asia: in Honor of Manuel Berberian's Forty-Five Years of Research Contributions. Geol. Soc. Spec. Publ. 525, 229–289. doi:10.1130/2016.2525(07).

Khan, S.R., Jan, M.Q., Khan, T., Khan, A.M., 2007. Petrology of the dykes from the Waziristan Ophiolite, NW Pakistan. J. Asian Earth Sci. 29, 369–377. doi:10.1016/j.jseaes.2006.08.001.

Kopp, C., Fruehn, J., Flueh, E.R., Reichert, C., Kukowski, N., Bialas, J., Klaeschen, D., 2000. Structure of the Makran subduction zone from wide-angle and reflection seismic data. Tectonophysics 329, 171–191. doi:10.1016/S0040-1951(00)00195-5.

Lachance, G.R., Trail, R.J., 1966. Practical solution to the matrix problem in X-ray analysis. Can. J. Appl. Spectrosc. 11, 43–48.
Lapierre, H., Samper, A., Bosch, D., Maury, R.C., Béchennec, F., Cotten, J., Demant, A., Brunet, P., Keller, F., Marcoux, J., 2004. The Tethyan plume: geochemical diversity of Middle Permian basalts from the Oman rifted margin. Lithos 74, 167–198.
Laws, E.D., Wilson, M., 1997. Tectonics and magmatism associated with Mesozoic passive continental margin development in the Middle East. J. Geol. Soc. London 154, 459–464.
Le Roex, A.P., Dick, H.J.B., Erlank, A.J., Reid, A.M., Frey, F.A., Hart, S.R., 1983. Geochemistry, mineralogy and petrogenesis of lavas erupted along the southwest Indian ridge between the Bouvet triple junction and 11 degrees east. J. Petrol. 24, 267–318. doi:10.1093/petrology/24.3.267.
Lustrino, M., Melluso, L., Morra, V., 2002. The transition from alkaline to tholeiitic magmas: a case study from the Orosei-Dorgali Pliocene volcanic district (NE Sardinia, Italy). Lithos 63, 83–113. doi:10.1016/S0024-4937(02)00113-5.
McCall, G.J.H., 1983. Mélanges of the Makran, southeastern Iran. In: McCall, G.J.H. (Ed.), Ophiolitic and Related Mélanges. Hutchinson Ross Publishing Company, Stroudsburg, Pennsylvania, pp. 292–299.
McCall, G.J.H., 1985a. Explanatory Text of the Fannuj Quadrangle Map 1. Geological Survey of Iran, Tehran, p. 416.
McCall, G.J.H., 1985b. Explanatory text of the Tahruie quadrangle map 1:250,000, geological quadrangle No. J 14. Heidary, Tehran (454 pp).
McCall, G.J.H., 1985c. Explanatory Text of the Minab Quadrangle Map 1:250,000, Geological Quadrangle No. J 13. Heidary, Tehran.
McCall, G.J.H., 1997. The geotectonic history of the Makran and adjacent areas of southern Iran. J. Asian Earth Sci. 15 (6), 517–531. doi:10.1016/S0743-9547(97)00032-9.
McCall, G.J.H., 2002. A summary of the geology of the Iranian Makran. The Tectonic and Climatic Evolution of the Arabian Sea Region, in: clift, P.D., Kroon, D., Gaedicke, C., Craig, J. (Eds.), The tectonic and climatic evolution of the Arabian sea region. Geol. Soc. Spec. Publ. Lond. 195, 147–204. doi:10.1144/GSL.SP.2002.195.01.10.
McCall, G.J.H., Kidd, R.G.W., 1982. The Makran southeastern Iran: the anatomy of a convergent margin active from Cretaceous to present. In: Leggett, J.K. (Ed.), Trench-Forearc Geology: sedimentation and Tectonics of Modern and Ancient Plate Margins, 10, pp. 387–397 Geol. Soc. Spec. Publ. Lond.
McCall, G.J.H., Eftekhar-Nezhad, J., Samimi-Namin, M., Arshadi, S., 1985. Explanatory text of the fannuj quadrangle map 1:250,000. In: McCall, G.J.H. (Ed.), Ministry of Mines and Metals. Geological Survey of Iran, Tehran.
Moghadam, H.S., Arai, S., Griffin, W.L., Khedr, M., Saccani, E., Henry, H., O'Reilly, S.Y., Ghorbani, G., 2022. Geochemical variability among stratiform chromitites and ultramafic rocks from Western Makran, South Iran. Lithos 412-413, 106591. https://doi.org/10.1016/j.lithos.2021.106591.
Mohammadi, A., Burg, J.-.P., Winkler, W., Ruh, J., von Quadt, A., 2016. Detrital zircon and provenance analysis of Late Cretaceous–Miocene onshore Iranian Makran strata: implications for the tectonic setting. Geol. Soc. Am. Bull. 128, 1481–1499. doi:10.1130/B31361.1.
Monsef, I., Rahgoshay, M., Pirouz, M., Chiaradia, M., Grégoire, M., Ceuleneer, G., 2019. The Eastern Makran Ophiolite (SE Iran): evidence for a Late Cretaceous fore-arc oceanic crust. Int. Geol. Rev. 61, 1313–1339. doi:10.1080/00206814.2018.1507764.
Moslempour, M.E., Khalatbari-Jafari, M., Ghaderi, M., 2015. Petrology, geochemistry and tectonics of the extrusive sequence of fannuj-maskutan ophiolite, southeastern Iran. J. Geol. Soc. India 85, 604–618. doi:10.1007/s12594-015-0255-y.
Pandolfi, L., Barbero, E., Marroni, M., Delavari, M., Dolati, A., Di Rosa, M., Frassi, C., Langone, A., Farina, F., MacDonald, C.S., Saccani, E., 2021. The Bajgan Complex revealed as a Cretaceous ophiolite-bearing subduction complex: a key to unravel the geodynamics of Makran (southeast Iran). J. Asian Earth Sci. 222, 104965. doi:10.1016/j.jseaes.2021.104965.
Pearce, J.A., 1996. A user's guide to basalt discrimination diagrams. In: Trace Element Geochemistry of Volcanic Rocks: applications for Massive Sulphide Exploration, 12. Geoscience Canada, pp. 79–113 Short Course Notes.
Pearce, J.A., 2008. Geochemical fingerprinting of oceanic basalts with applications to ophiolite classification and the search for Archean oceanic crust. Lithos 100, 14–48. doi:10.1016/j.lithos.2007.06.016.
Pearce, J.A., Norry, M.J., 1979. Petrogenetic implications of Ti, Zr, Y, and Nb variations in volcanic rocks. Contrib. Mineral. Petrol. 69, 33–47. doi:10.1007/BF00375192.
Photiades, A., Saccani, E., Tassinari, R., 2003. Petrogenesis and tectonic setting of volcanic rocks from the Subpelagonian ophiolitic mélange in the Agoriani area (Othrys, Greece). Ofioliti 28, 121–135.
Pirnia, T., Saccani, E., Torabi, G., Chiari, M., Gorican, S., Barbero, E., 2020. Cretaceous tectonic evolution of the Neo-Tethys in Central Iran: evidence from petrology and age of the Nain-Ashin ophiolitic basalts. Geosci. Front. 11, 57–81. doi:10.1016/j.gsf.2019.02.008.
Ricou, L.E., 1994. Tethys reconstructed: plates continental fragments and their boundaris since 260Ma from Central America to South-eastern Asia. Geodin. Acta 7, 169–218. doi:10.1080/09853111.1994.11105266.
Rolland, Y., Galoyan, G., Sosson, M., Melkonyan, R., Avagyan, A., 2010. The Armenian Ophiolite: insights for Jurassic back-arc formation, lower cretaceous hot spot magmatism and Upper cretaceous obduction over the South Armenian Block. Geol. Soc. Spec. Publ. Lond. 340, 353–382. doi:10.1144/SP340.15.
Rolland, Y., Hässig, M., Bosch, D., Bruguier, O., Melis, R., Galoyan, G., Topuz, G., Sahakyan, L., Avagyan, A., Sosson, M., 2020. The East Anatolia–Lesser Caucasus ophiolite: an exceptional case of large-scale obduction, synthesis of data and numerical modelling. Geosci. Front. 11, 83–108. doi:10.1016/j.gsf.2018.12.009.
Saccani, E., 2015. A new method of discriminating different types of post-Archean ophiolitic basalts and their tectonic significance using Th-Nb and Ce-Dy-Yb systematics. Geosci. Front. 6, 481–501. doi:10.1016/j.gsf.2014.03.006.
Saccani, E., Photiades, A., Padoa, E., 2003. Geochemistry, petrogenesis and tectonomagmatic significance of volcanic and subvolcanic rocks from the Koziakas Mélange (Western Thessaly, Greece). Ofioliti 28, 43–57. doi:10.4454/ofioliti.v28i1.189.
Saccani, E., Dilek, Y., Photiades, A., 2017. Time-progressive mantle-melt evolution and magma production in a Tethyan marginal sea: a case study of the Albanide-Hellenide ophiolites. Lithosphere 10, 35–53. doi:10.1130/L602.1.
Saccani, E., Delavari, M., Dolati, A., Marroni, M., Pandolfi, L., Chiari, M., Barbero, E., 2018. New insights into the geodynamics of Neo-Tethys in the Makran area: evidence from age and petrology of ophiolites from the Coloured Mélange Complex (SE Iran). Gondwana Res. 62, 306–327. doi:10.1016/j.gr.2017.07.013.
Saccani, E., Delavari, M., Dolati, A., Pandolfi, L., Barbero, E., Tassinari, R., Marroni, M., 2022. Geochemistry of basaltic blueschists from the Deyader Metamorphic Complex (Makran Accretionary Prism, SE Iran): new constraints for magma generation in the Makran sector of the Neo-Tethys. J. Asian Earth Sci. 228, 105141. doi:10.1016/j.jseaes.2022.105141.
Samimi Namin, M., 1982. Geological Map of Taherui 1: 250,000 Scale; Ministry of Mines and Metal. Geological Survey of Iran: Tehran, Iran.
Samimi Namin, M., 1983. Geological Map of Minab 1: 250,000 Scale; Ministry of Mines and Metal. Geological Survey of Iran: Tehran, Iran.
Sayit, K., 2013. Immobile trace element systematics of ocean island basalts: the role of oceanic lithosphere in creating the geochemical diversity. Ofioliti 38, 101–120.
Şengör, A.M.C., 1990. A new model for the Late Paleozoic-Mesozoic tectonic evolution of Iran and implications for Oman. In: The Geology and Tectonics of the Oman Region, 49. Geological Society Special Publication London, pp. 797–831. doi:10.1144/gsl.sp.1992.049.01.49.
Sepidbar, F., Lucci, F., Biabangard, H., Zaki Khedr, M., Jiantang, P., 2020. Geochemistry and tectonic significance of the Fannuj-Maskutan SSZ-type ophiolite (Inner Makran, SE Iran). Int. Geol. Rev. 62, 2077–2104. doi:10.1080/00206814.2020.1753118.
Shahabpour, J., 2010. Tectonic implications of the geochemical data from the Makran igneous rocks in Iran. Island Arc 19, 676–689. doi:10.1111/j.1440-1738.2010.00723.x.
Stampfli, G.M., Borel, G.D., 2002. A plate tectonic model for the Paleozoic and Mesozoic constrained by dynamic plate boundaries and restored synthetic oceanic isochrons. Earth Planet. Sci. Lett. 196, 17–33. doi:10.1016/S0012-821X(01)00588-X.
Sun, S.S., McDonough, W.F., 1989. Chemical and isotopic systematics of oceanic basalts: implications for mantle composition and processes. In: Magmatism in the Ocean Basins, 42. Geological Society Special Publication London, pp. 313–345. doi:10.1144/GSL.SP.1989.042.01.19.
Taylor, S.R., McLennan, S.M., 1985. The Continental Crust: Its Composition and Evolution. Blackwell, Oxford, p. 312.
Thirlwall, M.F., Upton, B.G.J., Jenkins, C., 1994. Interaction between continental lithosphere and the Iceland plume-Sr-Nd-Pb isotope geochemistry of Tertiary basalts, NE Greenland. J. Petrol. 35, 839–879. doi:10.1093/petrology/35.3.839.
Winchester, J.A., Floyd, P.A., 1977. Geochemical discrimination of different magma series and their differentiation products using immobile elements. Chem. Geol. 20, 325–343. doi:10.1016/0009-2541(77)90057-2.
Wood, D.A., 1980. The application of a Th-Hf-Ta diagram to problems of tectonomagmatic classification and to establishing the nature of crustal contamination of basaltic lavas of the British Tertiary volcanic province. Earth Planet. Sci. Lett. 50, 11–30. doi:10.1016/0012-821X(80)90116-8.
Workman, R.K., Hart, S.R., 2005. Major and trace element composition of the depleted MORB mantle (DMM). Earth Planet. Sci. Lett. 231, 53–72. doi:10.1016/j.epsl.2004.12.005.